Guo *et al. Energy Mater* 2024;4:400026
DOI: 10.20517/energymater.2023.82

Energy Materials

Review

Open Access

Advanced V-based materials for multivalent-ion storage applications

Weihua Guo, Danchen Fu, Huawei Song*, Chengxin Wang*

State Key Laboratory of Optoelectronic Materials and Technologies, School of Materials Science and Engineering, Sun Yat-Sen (Zhongshan) University, Guangzhou 510275, Guangdong, China.

***Correspondence to:** Prof. Chengxin Wang, State Key Laboratory of Optoelectronic Materials and Technologies, School of Materials Science and Engineering, Sun Yat-Sen (Zhongshan) University, Road Xingangxi No. 135, Haizhu District, Guangzhou 510275, Guangdong, China. E-mail: wchengx@mail.sysu.edu.cn; Prof. Huawei Song, State Key Laboratory of Optoelectronic Materials and Technologies, School of Materials Science and Engineering, Sun Yat-Sen (Zhongshan) University, Road Xingangxi No. 135, Haizhu District, Guangzhou 510275, Guangdong, China. E-mail: songhw5@mail.sysu.edu.cn

How to cite this article: Guo W, Fu D, Song H, Wang C. Advanced V-based materials for multivalent-ion storage applications. *Energy Mater* 2024;4:400026. https://dx.doi.org/10.20517/energymater.2023.82

Received: 23 Oct 2023 **First Decision:** 1 Dec 2023 **Revised:** 18 Dec 2023 **Accepted:** 1 Feb 2024 **Published:** 26 Mar 2024

Academic Editor: Hong Xu **Copy Editor:** Fangyuan Liu **Production Editor:** Fangyuan Liu

Abstract

Multivalent-ion batteries, as promising alternative or supplementary technologies to lithium-ion batteries, have increasingly attracted attention recently. Various advanced materials have been presented to pursue potential breakthroughs in energy and power. Among them, vanadium (V)-based materials benefiting from abundant resources, various polymorphs and valences, especially most with large interlayer spacings, are good candidates for multivalent-ion storage. However, limited by multiple inherent issues, e.g., strong electrostatic interactions, poor electronic conductivity, structure collapse or materials dissolution under battery operation, *etc.*, various strategies have sprung many advanced materials and applications and also brought about new challenges that are in urgent need to clarify and summarize. Hence, advanced V-based compounds developed for multivalent-ion storage in the past few years are selectively summarized and systematically analyzed, including vanadium oxides and sulfides, vanadates, and V-based MXenes and phosphates. Not only crystal structures and electrochemical properties but also mainstream ion storage mechanisms are critically reviewed. Through analyzing the challenges accompanying multivalent-ion storage, potential opportunities are anticipated.

Keywords: Multivalent-ion, charge storage, reaction mechanism, efficient energy storage

INTRODUCTION

With ever-growing need of energy storage and electric vehicles, various rechargeable batteries have gained much attention. Among them, lithium-ion batteries (LIBs) are currently dominating the global market for mobile power sources, but issues from safety, cost, and limited resources have hindered their further development[1-3]. Multivalent-ion batteries, such as Mg^{2+}, Ca^{2+}, Zn^{2+}, Al^{3+}, *etc.*, are attracting more and more interest due to their relatively high safety, considerable resource reserves, and good environmental friendliness[4-8]. However, multivalent ions carry more charges per ion than monovalent ions, which means a much stronger Coulomb interaction resulting in sluggish kinetics for ion diffusion[9]. Therefore, compared with monovalent-ion storage, it is much more crucial to search for suitable insertion hosts for efficient multivalent-ion storage.

There are many candidate electrodes, e.g., some layered oxides, Prussian blue analogs, organic compounds, *etc.*, appropriate for multivalent-ion storage, but they are generally challenged by issues such as poor cycling stability, inherent low capacity, severe dissolution, and so forth[10]. Among them, vanadium (V)-based compounds with abundant valences and rich resource reserves guarantee high theoretical capacity and cost-effective scale-application prospects[11,12]. Meanwhile, changeable V-O coordination chemistry of VO_4 tetrahedra, VO_5 triangular bipyramidal/square pyramidal, and VO_6 aberrant/ortho-octahedral and types of polymorphs and microstructures such as laminar, three-dimensional (3D) tunneling, chain, rock-salt structures, *etc.*, also offer a wide structure regulation freedom[12]. Crucially, most V-based compounds exhibit large interlayer spacings conducive to fast insertion/extraction of various multivalent ions. However, issues such as active material loss due to dissolution also occurred in some V-based compounds similarly[13]. Complex reaction mechanisms and low average operating voltage are also occasional challenges. Overall, V-based materials exhibited obvious advantages in emerging multivalent-ion storage. After years of rapid development, it is necessary to comprehensively review relevant achievements and discuss the challenges to present reasonable anticipation for future prospects and development trends. With this consideration, the manuscript systematically introduces the applications of different V-based compounds in various multivalent-ion batteries, as illustrated in Figure 1, including their crystal structure, electrochemical properties, and energy storage mechanism. Firstly, the structural characteristics and potential electrochemical applications of various V-based compounds will be discussed in Section "OVERVIEW AND CATEGORIES". Subsequently (Section "MULTIVALENT-ION STORAGE APPLICATION"), the electrochemical performance of Mg^{2+}, Ca^{2+}, Al^{3+}, and Zn^{2+} storage in non-aqueous or aqueous batteries, supercapacitors are separately reviewed, and especially, reaction mechanisms of Zn^{2+} are discussed to comb the emerging complex zinc (Zn) storage processes. Before the conclusion (Section "CONCLUSIONS AND FUTURE PROSPECTS"), various challenges of multivalent-ion storage for V-based materials are summarized, and their possible future trends and directions are predicated.

OVERVIEW AND CATEGORIES

Before introducing the Mg^{2+}, Ca^{2+}, Al^{3+} and Zn^{2+} multivalent-ion storage performance, various categories of V-based materials and their structures are summarized below. For simplification, they are generally divided as vanadium oxides (VO_x), vanadium sulfides (VS_x), vanadates (MVO_x), V-based phosphates ($MVPO_4$), and V-based MXenes (VXenes), respectively.

Vanadium oxides

Vanadium oxides show different valences of V from 0.4 to 5, forming a variety of symmetries such as triclinic V_4O_7, V_8O_{15}, V_7O_{13}, and V_6O_{11}, monoclinic VO_2 and V_2O_4, orthorhombic V_4O_9, tetragonal $VO_{0.2}$, $VO_{1.27}$ and V_2O_5, and cubic $VO_{0.9}$ and VO. They can typically be treated as corner-, edge-, or face-sharing V-O polyhedra with different oxygen coordination. Some common vanadium oxides [Figure 2] in energy

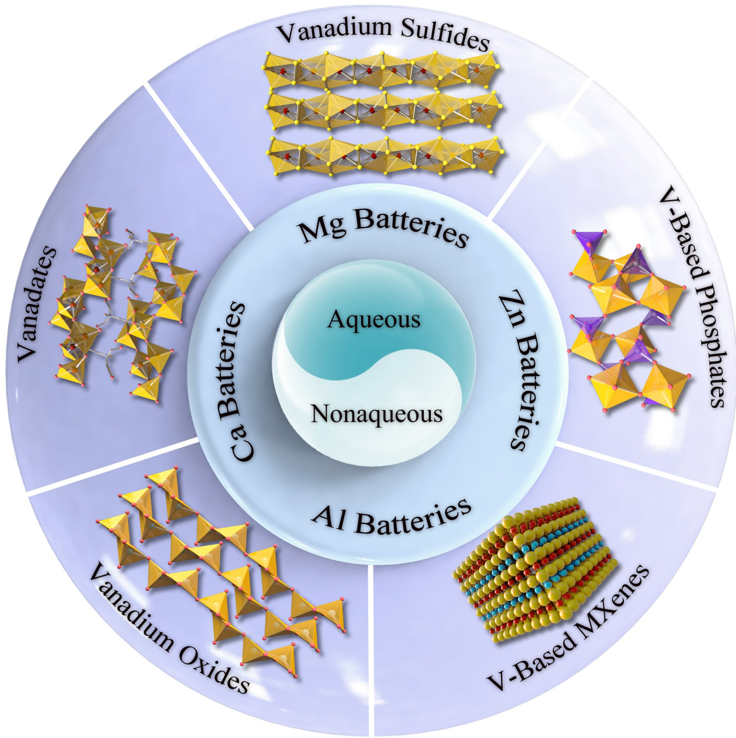

Figure 1. Illustration of V-based materials for multivalent-ion storage.

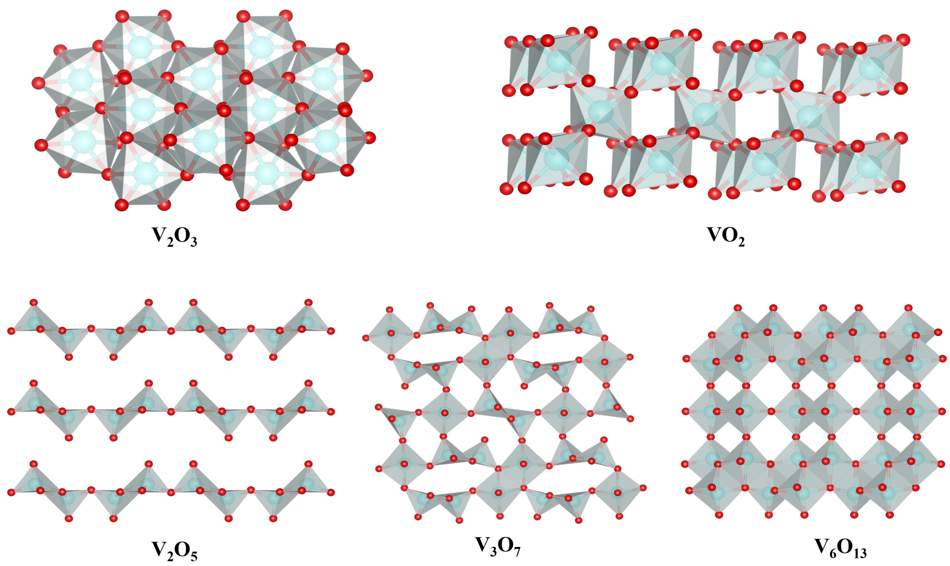

Figure 2. Structures of some typical vanadium oxides, O in red and V in cyan.

storage include octahedra, pentagonal bipyramid, square pyramid, and tetrahedra coordinated V_2O_5, VO_2, V_6O_{13}, V_2O_3, and V_3O_7[14]. Various valences and structures afford diverse multi-electron transfer chemistries and abundant vacancies needed for superior ion storage capability and fast kinetics for ion transport, especially for Mg^{2+}, Ca^{2+}, Zn^{2+}, and Al^{3+} multivalent ions[15,16]. However, unlike monovalent ions, multivalent ions generally exhibit strong Coulomb interaction with the host lattices, leading to considerable polarization and sluggish kinetics in mass and charge transfer processes. Meanwhile, poor electron conductivity and metastable structure of V-O polyhedral layers due to weak van der Waals bonding easily lead to serious capacity decay after repeatedly inserting/extracting multivalent ions. Various vanadium oxides still suffer from the problems of poor rate performance and serious capacity decay[17]. Hence, it is necessary to summarize and clarify their structure characteristics related to energy storage.

V_2O_5

V_2O_5, with V at the highest oxidation state of +5 which means a relatively larger charge storage capability, usually crystallizes into four polymorphs, i.e., orthorhombic, monoclinic, tetragonal, and orthorhombic. Among them, α-V_2O_5 is the most common polymorph with V-O square pyramid coordination forming a lamellar structure by co-orientation or co-angulation [VO_5] polyhedra[18]. The structure (Space group: *Pmnm*, a = 111.150 Å, b = 3.563 Å, and c = 4.370 Å) is usually thermodynamically stable[19]. It can be easy to regulate the weakly bonded lamellar structure to achieve fast insertion/extraction of different metal ions. However, the poor conductivities of both ions and electrons and intense host-guest interaction readily lead to significant volume change and easy polarization when V_2O_5 is used as a battery cathode. Thus, it is still difficult to achieve reversible and fast ion storage in pure V_2O_5[20].

VO_2

VO_2 can crystallize into more than a dozen phases, e.g., thermodynamically stable monoclinic VO_2(M), VO_2(B), and metastable tetragonal VO_2(A), VO_2(R)[21,22]. Among them, VO_2(B) exhibits much better performance for multivalent-ion storage[12]. VO_2(B) shows a layered structure consisting of [VO_6] octahedral bilayers, resembling a bilayered V_2O_5 structure with the removal of crystal water and interlayer collapse. Corner-shared [VO_6] octahedral bilayers in VO_2(B) contribute to abundant tunneling structures suitable for fast ion diffusion for multivalent-ion storage[23]. Moreover, the structure also counteracts lattice shear during the charging and discharging processes[24].

V_2O_3

V_2O_3 usually exhibits a rhombic corundum structure, characteristic of edge-sharing [VO_6] octahedra packed into a 3D tunnel structure, favorable for ion intercalation[25]. The structure belongs to the $R\bar{3}c$ space group (a = b = 4.9492(2) Å, c = 13.988(1) Å)[18]. Moreover, the electron conductivity of V_2O_3 is also superior to most transition metal oxides due to available V 3d electron transfer along the V-V chain[26].

V_6O_{13}

V_6O_{13} consists of alternating single- and double-twisted [VO_6] octahedral layers in a jagged arrangement containing mixed-valence V^{5+}/V^{4+}[23,27]. V_6O_{13} single- and double-twisted [VO_6] octahedral layers shared corners, showing a 3D open frame structure[28]. Based on valence bonding and calculations, only some of the vanadium sites in the bilayer show V^{5+} properties, while V^{4+} occupies the remaining vanadium sites[23].

V_3O_7

V_3O_7 is of mixed-valence V^{5+}/V^{4+} with an atomic ratio of 2:1, resulting in superior electrochemical properties compared to other vanadium oxides[12]. The crystal cell of V_3O_7 contains 36 vanadium atoms, 12 in octahedra and 24 in pentacoordination[18]. Its hydrate $V_3O_7·H_2O$ has a lamellar structure, consisting of V_3O_8 layers stacked along the a-axis with [VO_6] octahedral and [VO_5] square pyramid coordination by sharing corner/edge, and the H_2O molecules are distributed on both sides of the V_3O_8 layer. Adjacent layers are usually interconnected by hydrogen bonds, providing a buffer space due to the vibration of hydrogen bonds[29]. Therefore, during ion insertion/extraction, large lattice distortion can easily occur without destroying the crystal structure[30]. Compared to orthorhombic V_2O_5, $V_3O_7{\cdot}H_2O$ has a much larger layer spacing and is usually crystallized in a one-dimensional nanostructure[12].

Vanadium sulfides

Vanadium sulfide is available in many forms, e.g., VS_2, VS_4, V_2S_3, VS, V_2S_5, V_3S, and V_6S. Among them, VS_2 and VS_4 are usually used in batteries[31]. Their graphene-like structures afford large layer spacings, facilitating cation intercalation and diffusion. Vanadium atoms in VS_2 and VS_4 exhibit the same oxidation state, while sulfur atoms appear as S^{2-} monomers in VS_2 and S_2^{2-} dimers in VS_4, leading to entirely different physicochemical and electrochemical properties[32]. However, sulfides of vanadium are apt to be oxidized, especially when staying for a long duration in air atmosphere. This general phenomenon suggests that stringent conditions and atmosphere are essential for preparing or storing vanadium sulfide.

VS_2

VS_2 exhibits a lamellae structure similar to graphite. Each vanadium atom is linked to six sulfur atoms through covalent bonds, forming an S-V-S sandwich layer [Figure 3A] and weakly interlayer van der Waals bonding. The large interlayer spacing of 5.76 Å facilitates rapid ion diffusion and maintains structural integrity during repetitive cycling, making VS_2 a promising candidate for pseudocapacitance[33]. Compared to vanadium oxides, weakened electrostatic interactions in VS_2 result in a lower diffusion barrier for the cations, enabling reversible ion insertion/desertion. Additionally, VS_2 has good electrical conductivity, which, together with a low ion diffusion barrier, contributes to good performance for metal-ion batteries.

VS_4

VS_4 consists of parallel and one-dimensional atomic chain-like structures with bonding V^{4+} and S_2^{2-} dimer [Figure 3B], and the S_2^{2-} dimer affords enough ion storage sites. The open channels with a chain spacing of 5.83 Å favor the diffusion and storage of cations. However, pure VS_4 usually exhibits poor cycling performance and severe capacity degradation due to severe polarization, poor electron conductivity, and large volume expansion[34,35]. Various VS_4 nanostructures, such as nanoribbons, nanorods, nanocones, and nanosheets, have been synthesized and assembled into microspheres or layered structures as electrode materials for batteries to solve the above problems[36,37].

Vanadates

Vanadates usually show better electrochemical performance than vanadium oxides due to structure optimization effects of extra metal ions. Similar to $Zn_{0.25}V_2O_5$[38], many vanadates are made by inserting different cations into vanadium oxides, a strategy that preserves the rich chemical valence of the original vanadium oxide. Insertion of cations also increases the internal spacing of vanadium oxide, thus effectively mitigating the capacity loss. Furthermore, cations serve as pillars between layers, which prevents relative slip between adjacent V-O and supports both layers, stabilizing the V-O structure and avoiding vertical collapse[39]. According to the type of cations, vanadates can be divided into alkali metal and alkaline earth metal vanadate, transition metal vanadate, and other vanadates. Most vanadates were prepared using the hydrothermal method, so insertion of metal ions is usually accompanied by water molecules, forming vanadates with some crystallized water.

Alkali metal vanadates

LiV_3O_8 usually demonstrates good Li-storage performance[40]. Structures of NaV_3O_8 and LiV_3O_8 are similar, consisting of edge- or corner-sharing $[VO_6]$ octahedra layers, and Li^+ and Na^+ are located between the layers [Figure 3C]. Due to the large radius of K^+, it is impossible to form a similar structure. Differently, V_2O_8 units and VO_6 octahedra share edges and corners in KV_3O_8[41], two VO_5 square pyramids are connected by a VO_6 octahedron to form a $(V_3O_{12})_n$ chain stacked along the b-axis. Then, another reversed $(V_3O_{12})_n$ chain

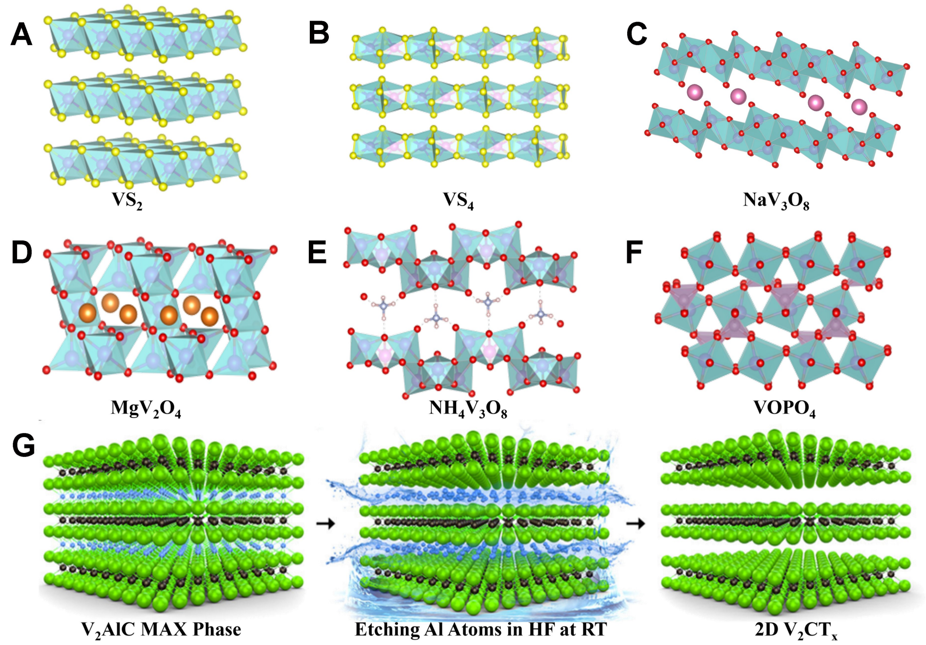

Figure 3. Structures of (A) VS_2, (B) VS_4, (C) NaV_3O_8, (D) MgV_2O_4, (E) $NH_4V_3O_8$, and (F) $VOPO_4$. (G) Illustration of selectively etching process to synthesize V_2CT_x MXene. Reproduced with permission[63]. Copyright 2017, American Chemical Society.

connects the above $(V_3O_{12})_n$ chains to form a KV_3O_8 layer along the b-axis[42]. $Li_3V_6O_{13}$ is also a typical alkali metal vanadate. It consists of octahedral $[VO_6]$ and triangular pyramidal $[VO_5]$ units shared on both sides, resembling strings and bands arranged along (110) crystal planes. Layer-structured octahedra and tetrahedra are connected by interstitial Li^+[43], forming a square cone ligand with five O atoms without occupying insertion sites of V_6O_{13}.

Alkali earth metal vanadates

MgV_2O_4, $Mg_xV_2O_5$, $CaV_6O_{16}\cdot 2.8H_2O$, *etc.*, are common alkaline earth metal vanadates reported for multivalent-ion storage. MgV_2O_4 consists of $[VO_6]$ octahedra and $[VO_4]$ tetrahedra, and Mg^{2+} can be inserted at the tetrahedral sites of the spinel oxide [Figure 3D]. The AV_2O_4-typed spinel (A = magnesium (Mg), calcium (Ca), *etc.*) is an attractive structure with which electrodes often exhibit abundant 3D channels, good crystal stability, tunable atomic scale structure, and suitable operating voltage[44]. The structure of $Mg_xV_2O_5\cdot nH_2O$ is similar to bilayer V_2O_5 that consists of $[VO_6]$ octahedra as the basic layer with Mg^{2+} or hydrated Mg^{2+} inserted between the layers[45]. The biotite talc $CaV_6O_{16}\cdot 2.8H_2O$ consists of a reconstructed α-V_2O_5 structure with layers comprising $[VO_5]$ square pyramids and $[VO_6]$ octahedra. The interlayered Ca^{2+} and water molecules raised the layer spacing from 4.37 to 8.10 Å and stabilized the interlayer structure[46].

Transition metal vanadates

Most ions of transition metals, e.g., Ag^+, Fe^{2+}/Fe^{3+}, Zn^{2+}, Co^{2+}, Cu^{2+}, Mn^{2+}/Mn^{3+}, Ni^{2+}, *etc.*, readily combine vanadium oxides to form the corresponding vanadates. $A_xV_2O_5\cdot nH_2O$ (A = Zn, manganese (Mn), Ni, Co, *etc.*) exhibits a layered structure similar to V_2O_5, with alternate $[VO_6]$ octahedral layer and hydrated cations between the layers[38,47]. ZnV_2O_4, akin to spinel MgV_2O_4, consists of $[VO_6]$ octahedra and $[VO_4]$ tetrahedra. Since the electrochemical performance of low-valent V-based oxides in aqueous solution is limited, researchers tend to oxidize ZnV_2O_4 electrochemically in the first few cycles, which leads to superior electrochemical performance[48]. Other transition metal vanadates include $FeVO_4$[49], $Cu_3V_2O_7(OH)_2\cdot H_2O$[50], CuV_2O_6[51], $ZnV_6O_{16}\cdot 8H_2O$[52], $Fe_2V_4O_{13}$[53], *etc.*, which are also reported efficient for multivalent-ion storage.

Other vanadates

Besides, aluminum (Al)-based and NH_4-based vanadates are relatively less studied. Actually, with a molecular weight relatively lower than that of transition metal vanadates, they generally deliver much larger specific capacities. Besides, insertion of Al^{3+} or NH_4^+ also makes the interlayer spacings larger and the ion conductivity higher, favoring the diffusion of metal ions[54]. With edge-shared twisted [VO_6] octahedra, the monoclinic $NH_4V_4O_{10}$ exhibits a stable bilayer structure. The NH_4^+ ion tends to act as a backbone cation to stabilize the structure, preventing severe volume changes during insertion of guest ions[55]. Hollow spheres of $H_{11}Al_2V_6O_{23.2}$ with a bilayer structure and low crystallinity showed little lattice distortion and good long-term cycling stability[56]. Crystallized $NH_4V_3O_8$ has a twisted zigzag layer structure consisting of VO_5 square cone units and twisted [VO_6] octahedra parallel to the (00l) plane, with NH_4^+ ions between the layers connecting with oxygen atoms through hydrogen bonding [Figure 3E][57].

V-based phosphates

A prominent feature of V-based phosphates is the output voltage higher than that of vanadates or vanadium oxides due to the inductive effect of the $(PO)_4^{3-}$ group[58]. Moreover, V-based phosphates also exhibit good structure stability and fast ion diffusion[58,59]. $VOPO_4$, $Na_3V_2(PO_4)_2F_3$, $Li_3V_2(PO_4)_3$, $Na_3V_2(PO_4)_3$, *etc*., are common explored V-based phosphates. $VOPO_4$ displays a typical layered crystal structure with vertex-sharing VO_6 octahedra and PO_4 tetrahedra in a 1:1 ratio [Figure 3F][60]. Hydrothermal synthesized $VOPO_4$ tends to form the hydrate $VOPO_4{\cdot}nH_2O$, which easily decomposes into VO_x during cycling, so the cycling performance is poor[61]. The 3D framework of $Na_3V_2(PO_4)_3$ cathode consists of strongly bonded tetrahedral [PO_4] and octahedral [VO_6] units with large gaps, favoring fast ion transport. However, due to the poor electron conductivity, $Na_3V_2(PO_4)_3$ is often doped with metal ions or coated with conductive carbon to improve the conductivity. The introduction of highly electronegative F^- in $Na_3V_2(PO_4)_3$ can further increase the operating voltage[62]. Stable V-F bonding in the skeleton facilitates the formation of a new polyanion system, further enhancing its inductive effect. $Na_3V_2(PO_4)_2F_3$ consists of [$V_2O_8F_3$] double octahedra with [VO_4F_2] octahedra sharing corners with [PO_4] tetrahedra through an F atom, while [VO_4F_2] octahedra are connected to [PO_4] tetrahedra through O atoms, and sodium (Na) is located in the a-axis and b-axis in the position of open tunnels. Alignment and stacking in the $Na_3V_2(PO_4)_2F_3$ framework provide many channels that offer convenient ion diffusion paths. However, similar to most phosphates, they also exhibit very poor electronic conductivity and low capacity[60].

V-based MXenes

MXenes (M and X stand for an early transition metal and C/N elements, respectively) represent a series of two-dimensional (2D) inorganic compounds comprising several atomic layers of transition metal carbides, nitrides, or carbon-nitrides. They are typically produced by selectively removing metal ions in the A layer in the MAX phase with a combination of HF or LiF/HCl aqueous solution as etchants [Figure 3G][63]. Meanwhile, they also exhibit extraordinary physical, chemical, and electrochemical properties, such as hydrophilic surfaces, ultra-high electrical conductivity, and accordion-like laminate structure, making MXenes a good candidate to form a series of functional composites[64]. The primary four types of MXenes are titanium, niobium, vanadium, or molybdenum-based. Among them, most studies are Ti-based MXenes with large interlayer spacings, and abundant active sites allow for fast insertion/extraction of various guest ions[65]. However, the non-environmentally friendly preparation mostly involves harmful and hazardous HF, limiting the application of MXenes. Currently, V_2CT_x (T_x representing different surface functional groups) is the widely used V-based MXenes in multivalent-ion batteries[63], which undergoes multi-electron redox reactions. Due to its low valence of V (+2 and +3), it usually exhibits a relatively low capacity. To enhance the ion storage capability, *in situ* electrochemical activation was used to increase the valence state of V in

V_2CT_x while preserving its V-C-V 2D layered structure[66]. In addition, V-based MXenes were also ideal supports to form composite electrode materials with $Mg_{0.2}V_2O_5 \cdot nH_2O$[67], VS_4[68], and other V-based compounds for multivalent-ion storage.

MULTIVALENT-ION STORAGE APPLICATION

Non-aqueous batteries

Batteries with non-aqueous electrolytes usually exhibit a much wider electrochemical window and higher energy density than aqueous ones. However, active metal anodes in organic electrolytes tend to form insulative and passivated interphases, resulting in sluggish ion transport. It is a significant obstacle to reversible plating/stripping processes for Mg-/Ca-metal batteries. Differently, the ion diffusion rate in aqueous electrolytes is faster than in organic ones due to the fact that water has a charge shielding effect which can reduce the polarization of ions to the host lattice[69]. Therefore, small amounts of water are sometimes introduced into the organic electrolytes to reduce polarization and improve the reaction kinetics by obtaining a charge-shielding effect or converting metal ions into low-polarized solvated ions.

Mg-metal batteries

With many virtues of Mg, such as rich natural abundance, high capacity, low redox potentials, *etc.*, Mg-metal batteries have been intensively explored. Aurbach *et al.* reported the first highly reversible rechargeable magnesium battery system using Mo_6S_8 as the cathode in 2000[69]. However, the low capacity and discharge voltage of Chevel-phase Mo_6S_8 limit further development. So far, many electrode materials have been explored, such as transition metal sulfides[69], transition metal oxides[70], polyanionic compounds[71], and organic materials[72] for Mg-storage. Among them, V-based materials, with abundant valence states and unique layered structures or open backbones favoring reversible insertion/extraction of considerable Mg^{2+} ions, have been increasingly attractive. However, strong Mg-host interactions due to inherent divalent charge and large radius cause severe ion polarization, which is one of the main reasons hindering the application of V-based compounds.

To alleviate the relevant issues of inherent small layer spacings and strong electrostatic interactions, strategies, such as pre-intercalating large organic ions, adding electrolyte additives or surfactants, doping, *etc.*, have been frequently investigated. Through intercalating large organic cation of $C_{10}H_{22}N^+$ in the first discharge, the interlayer spacing of VS_2 was significantly enlarged, raising the diffusion coefficient of Mg^{2+} to 10^{-10}-10^{-12} cm^{-2} s^{-1}[73]. Thus, the corresponding cathode of VS_2 nanosheets achieved a large capacity of 299 mAh g^{-1} at 50 mA g^{-1}. Besides, a capacity of 214 mAh g^{-1} was retained even at 2.0 A g^{-1}. The spontaneous agglomeration of VS_4 was prevented by using surfactants or special self-assembly, leading to unique flower-like or sea urchin-like morphologies that afford abundant surfaces/interfaces and voids for stable Mg^{2+} intercalation/deintercalation[74]. In addition, S_2^{2-} dimers in the chain-like crystal structure of VS_4 also provide abundant sites for Mg-storage[75]. The introduction of dopants such as Mo to replace V would result in the escape of isolated S, then creating abundant S vacancies in a Mo-doped VS_4 cathode. At 50 mA g^{-1}, a Mg-storage capacity of 120 mAh g^{-1} was attained at an optimized Mo content of 3% (atomic ratio)[76].

In most cases, Mg-storage in vanadium sulfides is based on the Mg^{2+} intercalation mechanism, but intercalation of complexion ions, e.g., $MgCl^+$, has also been frequently disclosed. For example, through both theoretical and experimental studies, Pei *et al.* found that $MgCl^+$ reversibly intercalated into/deintercalated out of VS_4@reduced graphene oxide (rGO) rather than Mg^{2+} when 0.25 M $[Mg_2Cl_3]^+[AlPh_2Cl_2]^-$/tetrahydrofuran was used as the electrolyte, contributing to 268.3 mAh g^{-1} at 50 mA g^{-1}[77]. Zhu *et al.* also observed reversible intercalation/deintercalation of $MgCl^+$ in VS_4 nanosheets /carbon-coated Ti_3C_2-MXenes hybrid cathodes[68]. The presence of V-C bonding proved a strong coupling between VS_4 and Ti_3C_2, and this unique layered nano-microstructure improved the accessibility of electrolytes, which reduces resistance of charge transfer. So, the hybrid delivered 492 mAh g^{-1} at 50 mA g^{-1}. After 900 cycles, it also held 80% capacity retention at 0.5 A g^{-1}. In addition, co-intercalation of Mg^{2+} and $MgCl^{+}$ also happened to some vanadium sulfides. For example, 2-methylhexanamine *in situ* intercalated VS_2 with a large layer spacing of 9.93 Å reversibly intercalated/deintercalated Mg^{2+} and $MgCl^{+}$, as shown in the corresponding XPS and EDS characterization [Figure 4A-C][78]. A polyvinylpyrrolidone/VS_4 composite was also found to simultaneously intercalate Mg^{2+} and $MgCl^{+}$[79].

Compared to vanadium sulfides, the high electronegativity of oxygen leads to higher ionic character of V-O bonding in the oxides, and the strengthened bonding usually raises the electrochemical potential for metal-ion intercalation. Moreover, higher voltage and lower molecular weight will increase the specific energy. For example, monodispersed V_2O_5 hierarchical spheres delivered good performance of 190 mAh g^{-1} at 10 mA g^{-1}[80] because irreversible Mg^{2+} intercalation at the initial charge/discharge process acted as a pillar in the interlayer of V_2O_5.

However, pure V_2O_5 is severely confined for Mg-storage because of poor ion and electron transport processes. It is efficient to improve the conductivity by intercalating electron conductive organics. For example, a 2D organic-inorganic superlattice with alternately arranged monolayered V_2O_5 nanosheets and polyaniline (PANI) monolayers exhibited a Mg-storage capacity of 270 mAh g^{-1} at 100 mA g^{-1}, far superior to only 102 mAh g^{-1} of pure V_2O_5 under the same testing conditions. Benefiting from the π-π conjugated chains, monolayer PANI not only served as pillars to enlarge layer spacings but also functioned as electron conducting pathways and active sites for Mg-storage[81]. Another V_2O_5/PEDOT (3,4-ethylene dioxythiophene) hybrid cathode achieved 348.3 mAh g^{-1} at 100 mA g^{-1} due to a widened interlayer spacing of 19.2 Å about 4.37 times that of pure V_2O_5[82]. Besides, it is also effective to improve the kinetics of V_2O_5 by introducing oxygen vacancies. An O-vacancy riched Ti-V_2O_{5-x} with a honeycomb structure exhibited an impressive electronic conductivity six times higher than that of pure V_2O_5. Due to the improved kinetics, the O-vacancy riched electrode delivered a Mg-storage capacity of 245.4 mAh g^{-1} at 100 mA g^{-1}, except for 79.6% retention after 400 cycles[83].

Pre-intercalation of metal ions into vanadium oxides also enhances the Mg-storage performance. For example, V_3O_8 with hydrothermally intercalated Li^{+}, Na^{+} and K^{+} ions delivered different Mg-storage capacities of 252.2, 204.16 and 37.56 mAh g^{-1} at 100 mA g^{-1}, respectively, [Figure 4D] except for the capacity retention of 42.2%, 85.78%, and 88.6% [Figure 4E], respectively, after 30 cycles[84]. The V-O layer spacing at different charging and discharging stages does not recover to be the same as the initial [Figure 4F]. Some Mg^{2+} may remain in the interlayers and gradually accumulate during the cycling process, resulting in poor cycling performance. Other metal-ion intercalated vanadium oxides, e.g., $Mg_{0.3}V_2O_5·1.1H_2O$, $Mn_{0.04}V_2O_5·1.17H_2O$, $Mn_{0.04}V_2O_5·1.17H_2O$, NaV_6O_{15}, *etc.*, were also reported with better Mg-storage performance than their parent oxides.

Although interlayer structures of vanadium oxides can be stabilized with intercalated metal ions, the effects of space charge repulsion and occupied active sites by pre-intercalated ions will reduce initial capacities. Differently, water molecules can effectively widen the interlayer spacings and buffer the charge repulsion effect between guest ions and elements from the host structures. There are two common strategies to introduce water molecules. One is *in-situ* formation of active materials with crystal water in an aqueous solution, and the crystal water acts as both interlayer support and charge shielding layers. The hydrothermally synthesized $NaV_3O_8·1.69H_2O$ nanoribbons exhibited a Mg-storage capacity of 110 mAh g^{-1} at 10 mA g^{-1}, which decays rapidly due to fast Mg consumption from leaching crystal water[85]. Second, trace

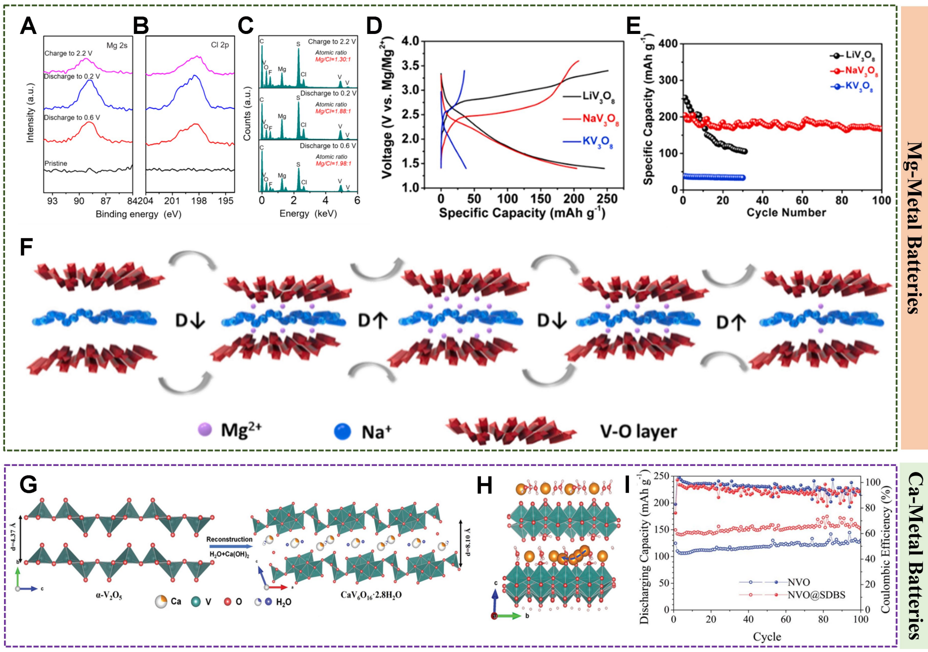

Figure 4. XPS spectra of (A) Mg 2s, (B) Cl 2p, and (C) EDS spectra for expanded VS_2 electrodes. Reproduced with permission[78]. Copyright 2019, Wiley-VCH GmbH. (D) Charge-discharge curves (A = Li, Na, K) and (E) cycling performance of A-V_3O_8 (A = Li, Na, K) at 100 mA g^{-1}, and (F) spacing change of NaV_3O_8 at different charge-discharge stages. Reproduced with permission[84]. Copyright 2019, Elsevier. (G) Formation of $CaV_6O_{16}\cdot 2.8H_2O$ and (H) Ca-storage in $CaV_6O_{16}\cdot 2.8H_2O$. Reproduced with permission[178]. Copyright 2022, Wiley-VCH GmbH. (I) Cycling performance of Zr-$NH_4V_4O_{10}$ at 0.2 A g^{-1}. Reproduced with permission[92]. Copyright 2022, Elsevier.

amounts of water in organic electrolytes can be more ion-conductive. Meanwhile, it does not lower the electrochemical stabilization windows. For example, $NaV_8O_{20}\cdot nH_2O$ in mixed solvents of tetramethylene glycol dimethyl ether (TEGDME)/water (4:1 by volume) delivered much better performance than that in pure TEGDME (351 mAh g^{-1} *vs.* 169 mAh g^{-1} at 0.3 A g^{-1}), except for a wide window voltage of 3.9 V[86]. Joe *et al.* improved the diffusion coefficient of 0.3 M Mg $(TFSI)_2$/AN electrolyte up to 2.45 times by adding 3 M water[82].

As to V-based phosphates, pre-intercalation of small molecules of H_2O or organics was also explored to improve the Mg-storage performance. For example, water or aniline molecules enhanced the diffusion kinetics of $VOPO_4$ cathodes due to widened interlayer spacings. Benefiting from a fast $MgCl^+$ intercalation mechanism, the cathode delivered 310 mAh g^{-1} at 50 mA g^{-1} and 192 mAh g^{-1} at 0.1 A g^{-1} even after 500 cycles[87]. Similarly, the metal-ion pre-intercalated cathode of $Li_3V_2(PO_4)_3$ composite delivered 124 mAh g^{-1} at 0.1 A g^{-1} and 80% capacity retention after 300 cycles at 0.5 A g^{-1} in an organic electrolyte with 1.5% water content. Mechanism characterization disclosed that Li^+ was extracted from the cathode during the first charge and co-intercalated with Mg^{2+} in subsequent cycles, contributing to an enhanced storage capacity[88]. Table 1 presents a direct comparison of the electrochemical performance of some representatives.

Ca-metal batteries

The lower reduction potential of Ca (-2.87 V *vs.* SHE) than Mg allows its metal batteries to deliver much higher voltages. Meanwhile, the lower charge density and polarization also contribute to better diffusion kinetics. However, various vanadium oxides suffered severe structural degradation and collapse during ion insertion/extraction. The derivatives with pre-intercalated metal ions, e.g., $A_xV_2O_5\cdot nH_2O$, where A stands for

Table 1. Performance comparison of V-based materials for multivalent-ion batteries

Materials	Application	Electrolyte	Capacity (mAh g^{-1})	Cycle performance
NaV_6O_{15} [179]	MIB	0.5 M $Mg(ClO_4)_2$/AN	137 (0.05 A g^{-1})	80%, 10 mA g^{-1} (100 cycles)
$Mg_{0.3}V_2O_5{\cdot}1.1H_2O$ [16]	MIB	0.3 M Mg $(ClO_4)_2$/AN	164 (0.1A g^{-1})	80%,2 A g^{-1} (10,000 cycles)
$FeVO_4$ [49]	MIB	0.3 M $Mg(ClO_4)_2$/AN	270 (0.5 A g^{-1})	85%,1 A g^{-1} (10,000 cycles)
$H_{11}Al_2V_6O_{23.2}$ [180]	MIB	0.3 M $Mg(ClO_4)_2$/AN	165 (0.1 A g^{-1})	87%,1 A g^{-1} (3,000 cycles)
$Li_3V_2(PO_4)_3$ [88]	MIB	0.3 M $Mg(ClO_4)_2$/PC	124 (0.1 A g^{-1})	80%,0.5 A g^{-1} (300 cycles)
VS_2 [73]	MIB	0.4 M APC-$PP_{14}Cl$/THF	214 (2 A g^{-1})	78%,1 A g^{-1} (300 cycles)
$Mn_{0.04}V_2O_5{\cdot}1.17H_2O$ [181]	MIB	0.3 M $Mg(ClO_4)_2$/AN	145 (0.05 A g^{-1})	82%,1 A g^{-1} (10,000 cycles)
$CaV_6O_{16}{\cdot}2.8H_2O$ [46]	CIB	$Ca(TFSI)_2/G_2$	134.7 (0.1 A g^{-1})	75%,0.1 A g^{-1} (50 cycles)
$Mg_{0.25}V_2O_5{\cdot}H_2O$ [182]	CIB	0.8 M $Ca(TFSI)_2$ in carbonate	120 (0.02 A g^{-1})	86.9%,0.5 A g^{-1} (500 cycles)
$Ca_{0.28}V_2O_5{\cdot}H_2O$ [90]	CIB	0.5 M $Ca(ClO_4)_2$/PC	142 (0.01 A g^{-1})	74%,0.03 A g^{-1} (50 cycles)
$K_2V_6O_{16}{\cdot}2.7H_2O$ [114]	CIB	5 M $Ca(NO_3)_2$	114 (0.02 A g^{-1})	78.5%,0.05 A g^{-1} (100 cycles)
$NH_4V_4O_{10}$ [92]	CIB	0.25 M $Ca(TFSI)_2$/PC	77 (0.05 A g^{-1})	89%,0.2 A g^{-1} (500 cycles)
$Ca_{0.26}V_2O_5{\cdot}H_2O$ [89]	CIB	0.8 M $Ca(TFSI)_2$ in carbonate	196 (0.02 A g^{-1})	93.6%,1 A g^{-1} (2,500 cycles)
$FeV_3O_9{\cdot}1.2H_2O$ [183]	CIB	0.5 M $Ca(ClO_4)_2$/AN	96 (0.2 A g^{-1})	79%,0.2 A g^{-1} (400 cycles)
$Li_2V_6O_{13}$ [96]	AIB	[EMIm]Cl:$AlCl_3$ = 1:1.3	159 (0.1 A g^{-1})	73%,0.05 A g^{-1} (300 cycles)
VS_4 [98]	AIB	[EMIm]Cl:$AlCl_3$ = 1:1.3	408 (0.1 A g^{-1})	39%,0.5 A g^{-1} (500 cycles)
V_2O_5 [184]	ZIB	2 M $ZnSO_4$	425 (0.3 A g^{-1})	78.5%,3 A g^{-1} (200 cycles)
VO_2 [185]	ZIB	3 M $Zn(CF_3SO_3)_2$	280 (0.1 A g^{-1})	86%,3 A g^{-1} (5,000 cycles)
V_3O_7 [186]	ZIB	2.5 M $Zn(CF_3SO_3)_2$	233 (0.2 A g^{-1})	96.2%,2 A g^{-1} (1,120 cycles)
V_6O_{13} [28]	ZIB	3 M $Zn(CF_3SO_3)_2$	360 (0.2 A g^{-1})	92%,4 A g^{-1} (2,000 cycles)
V_2O_3 [140]	ZIB	3 M $Zn(CF_3SO_3)_2$	196 (0.1 A g^{-1})	81%,5 A g^{-1} (30,000 cycles)
VS_2 [127]	ZIB	1 M $ZnSO_4$	187 (0.1 A g^{-1})	80%,2 A g^{-1} (2,000 cycles)
VS_4 [130]	ZIB	2 M $Zn(CF_3SO_3)_2$	265 (0.25 A g^{-1})	93%,5 A g^{-1} (1,200 cycles)
$NH_4V_4O_{10}$ [187]	ZIB	3 M $Zn(CF_3SO_3)_2$	298 (0.1 A g^{-1})	89%,2 A g^{-1} (2,000 cycles)
LiV_3O_8 [188]	ZIB	3 M $Zn(CF_3SO_3)_2$	298 (1 A g^{-1})	85%,5 A g^{-1} (4,000 cycles)
$Na_{0.33}V_2O_5$ [189]	ZIB	3 M $Zn(CF_3SO_3)_2$	367 (0.1 A g^{-1})	93%,1 A g^{-1} (1,000 cycles)
$Mg_{0.2}V_2O_5$ [67]	ZIB	3 M $Zn(CF_3SO_3)_2$	346 (0.1 A g^{-1})	83.7%,5 A g^{-1} (10,000 cycles)
ZnV_3O_8 [190]	ZIB	3 M $Zn(CF_3SO_3)_2$	294 (0.1 A g^{-1})	74.6%,2 A g^{-1} (1,200 cycles)
$Fe_2V_4O_{13}$ [53]	ZIB	2 M $Zn(CF_3SO_3)_2$	380 (0.2 A g^{-1})	83%,10 A g^{-1} (1,000 cycles)
$Na_3V_2(PO_4)_2F_3$ [191]	ZIB	2 M $Zn(CF_3SO_3)_2$	60 (0.2 A g^{-1})	95%,1 A g^{-1} (4,000 cycles)

metal ions, exhibited good structural stability in Ca-storage. At a testing temperature of 50 °C, reversible capacities of 142.4, 109.8, and 86.6 mAh g^{-1} were obtained in $Mg_{0.25}V_2O_5{\cdot}H_2O$, $Ca_{0.26}V_2O_5{\cdot}H_2O$, and $Sr_{0.42}V_2O_5{\cdot}0.7H_2O$ cathodes after 60 cycles at 100 mA g^{-1}[89]. The former two cathodes suffered from mono-phase solid-solution reactions during Ca^{2+} insertion/extraction, while the latter performed a two-phase transformation reaction. A similar $Ca_{0.28}V_2O_5{\cdot}H_2O$ cathode was reported to suffer from an initial irreversible amorphization before reversible insertion/extraction of Ca ions, which afforded 143 mAh g^{-1} at 10 mA g^{-1}[90]. Moreover, some metal-ion intercalated vanadium oxides also followed a Ca-storage-like ion exchange mechanism. $K_{0.5}V_2O_5$ transformed into $Ca_{0.45}V_2O_5$, contributing a reversible capacity of 65 mAh g^{-1} at 66.6 mA g^{-1} and high capacity retention of 92% after 100 cycles[91].

In addition to oxide derivatives with pre-inserted metal ions, vanadates, such as $CaV_6O_{16}{\cdot}2.8H_2O$[46], are also good candidates for Ca-storage. $CaV_6O_{16}{\cdot}2.8H_2O$ showed capacities of 175.2 mAh g^{-1} at 50 °C and 131.7 mAh g^{-1} at room temperature. Ca^{2+} undergoes a solid-solution reaction [Figure 4G] with a diffusion barrier of 0.36 eV along the b-direction [Figure 4H]. A Na-doped $NH_4V_4O_{10}$ cathode with rod-shaped particles initially discharged 125 mAh g^{-1} at 0.1 A g^{-1}[55]. Another Zr-doped $NH_4V_4O_{10}$ initially discharged 78 mAh g^{-1} at 50 mA g^{-1} [Figure 4I], showing a discharge voltage of about 3.0 V *vs.* Ca^{2+}/Ca[92]. The performance of them is also compared in Table 1.

Al-/Zn-metal batteries

Rechargeable aluminum batteries (RABs) have been intensively focused due to their high safety and rich aluminum abundance[93]. However, they still face many issues, such as severe corrosion of liquid electrolytes, significant volume change, low discharge voltage, poor reversibility, and so on[94,95]. Wang *et al.* reported that a $FeVO_4$@ PANI nanoribbon composite held 300 mAh g^{-1} after 300 cycles at 0.3 A g^{-1}[93]. Besides, it achieved 268.6 mAh g^{-1} after 200 cycles, even at a low temperature of -10 °C. A pre-lithium vanadium oxide derivative of $Li_2V_6O_{13}$ attained 161.6 mAh g^{-1} at 50 mA g^{-1} after 300 cycles, far superior to that of pristine V_6O_{13} whose capacity rapidly decays to 45.4 mAh g^{-1} after 50 cycles[96]. Transition metal sulfides, e.g., VS_4 in nanowires or auricular shapes, were also reported to deliver good Al-storage performance. A channel-rich VS_4 nanowire achieved 252.5 mAh g^{-1} at 100 mA g^{-1} after five activation cycles and held 138.9 mAh g^{-1} after 100 cycles at 0.4 A g^{-1}[97]. An auricular VS_4 retained 322.2 mAh g^{-1} at 200 mA g^{-1} after 120 cycles[98]. However, they displayed quite different ion storage mechanisms. Furthermore, the V_2CT_x MXenes electrode also demonstrated good Al-storage capacity exceeding 300 mAh g^{-1} at 100 mA g^{-1}[63].

Metallic zinc is also a safe anode. However, the research on Zn-metal batteries in organic electrolytes is limited due to lower voltages and capacities. A flower-like $NH_4V_4O_{10}$ attained a capacity of 486 mAh g^{-1} at 0.1 A g^{-1} in 1 M Zn $(ClO_4)_2$/propylidene carbonate (PC) electrolyte [Figure 5A], which displayed little capacity decay at 10 A g^{-1} for 3,000 cycles [Figure 5B][99]. With the same electrolyte, a paper-like electrode with perfectly aligned $Na_2V_6O_{16}\cdot 3H_2O$ nanoribbons exhibited 216 mAh g^{-1} at 0.5 A g^{-1}, and 167 mAh g^{-1} was still attained at 5 A g^{-1} after 5,000 cycles[100]. Besides, a composite with $V_2O_5\cdot 1.6H_2O/Ti_3C_2$ MXenes heterostructured nanosheets delivered 205.5 mAh g^{-1} at 0.1 A g^{-1} in triethyl phosphate electrolyte with a trace of water, and capacity retention of 78.6% was obtained at 0.5 A g^{-1} after 4,000 cycles[101]. The performance is also compared in Table 1.

Hybrid-ion batteries

Considering the limitations of single-ion storage, e.g., safety issues and high cost of lithium, high polarization of Mg^{2+}, hybrid-ion storage has attracted increasing attention in recent years[102]. For example, in a Mg/Li hybrid electrolyte, Li^+ dominates the cathode insertion because the diffusion rate of Li^+ in the cathode is much larger than that of Mg^{2+}. At the discharge, Mg^{2+} ions are dissolved from the Mg anode, while Li^+ ions are inserted into the cathode [Figure 5C][103]. Meanwhile, in the charge process, the situation is just the opposite. A hybrid Mg-Li-ion battery combines the advantages of a Mg anode without dendrite deposition and a fast lithium insertion cathode, making it a better alternative to LIBs for power storage[104].

Layered V-based compounds are good ion intercalation hosts due to their large specific capacity and multi-electronic reactions. For example, the hybrid batteries of Mg^{2+}/Na^+ and Mg^{2+}/K^+ with VS_2 cathodes were also explored. It was observed that ions of Li^+, Na^+, or K^+ could be co-inserted with Mg^{2+} into VS_2. Differently, co-insertion of Mg^{2+}/Li^+ or Mg^{2+}/K^+ led to the collapse of VS_2, while Mg^{2+}/Na^+ reversibly co-intercalated into VS_2, contributing to a capacity of 170 mAh g^{-1} at 0.1 A g^{-1} and 96.5% retention after 1,000 cycles[105]. A Mg^{2+}/Li^+ battery with a graphene-wrapped VS_2 cathode and a Mg anode delivered 235 mAh g^{-1} at 90 mA g^{-1}, and about 146 mAh g^{-1} was held at 9.5 A g^{-1} after 10,000 cycles [Figure 5d] [103]. The mechanism of a Mg^{2+}/Li^+ hybrid-ion battery with a $NaV_3O_8\cdot 1.69H_2O$ cathode revealed Li^+ insertion/extraction at the cathode was accompanied by a small amount of Mg^{2+} adsorption, while the anode is dominated by Mg^{2+} deposition/dissolution[106]. Differently, both Mg^{2+} and Li^+ were involved in the cathodic intercalation reaction and accompanied by a change in the valence state of Mo/V in another V_2MoO_8 cathode[17]. In a Ca^{2+}/Zn^{2+} hybrid-ion battery using a $Na_3V_2(PO_4)_3$ cathode, the open framework in the cathode achieves fast

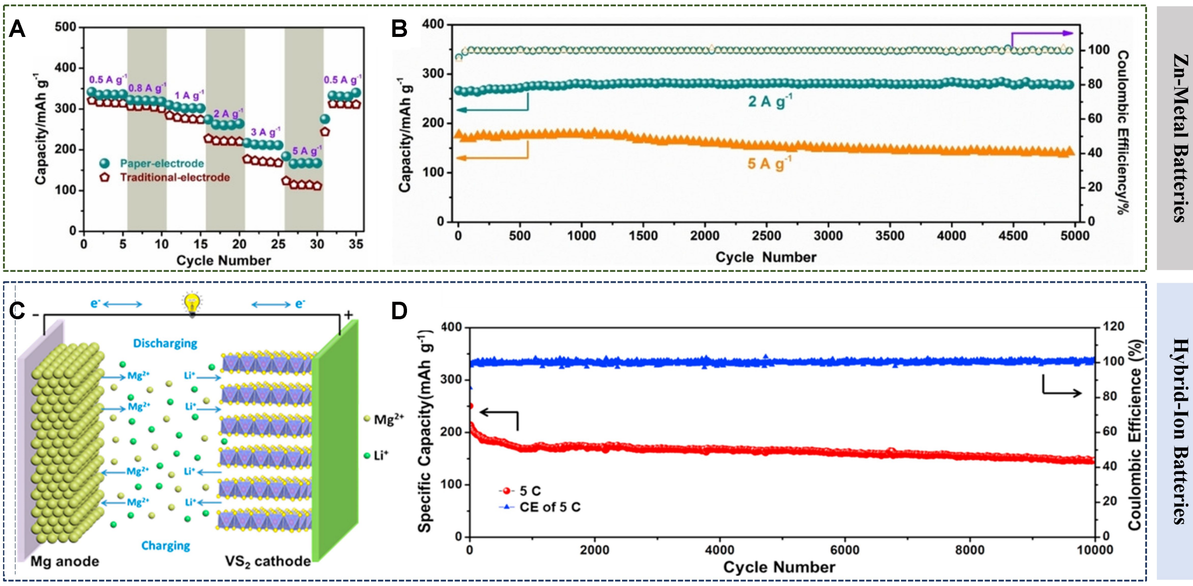

Figure 5. (A) Rate and (B) long-term cycling performance of $Na_2V_6O_{16}{\cdot}3H_2O$. Reproduced with permission under the terms of the Creative Commons Attribution[99]. Copyright 2020, the Author(s), Springer Nature. (C) Working mechanism and (D) cycling performance of VS_2-GO. Reproduced with permission[103]. Copyright 2018, Elsevier.

kinetics and good cycling stability for Ca^{2+} storage, and Ca^{2+} preferentially adsorbed on the zinc anode to form an electrostatic shielding layer, which inhibited zinc dendrites and improved the cycling performance[107].

Aqueous batteries

Compared with organic electrolytes, aqueous electrolytes, benefiting from good conductivity, low cost, high safety, *etc.*, have attracted intensive attention in energy storage[108]. The multivalent metal-ion storage of V-based compounds in aqueous electrolytes is discussed in the following.

Mg-/Ca-ion batteries

The available electrode materials for aqueous Mg-ion batteries have faced issues such as limited storage capability due to sluggish Mg-ion diffusion kinetics, easy structure degradation accompanying Mg-ion intercalation resulting from large volume effect and dissolution of active materials, *etc.* Therefore, relevant references are much less than those about non-aqueous batteries. Zhang *et al.* used VO_2 as an anode and 1.0 M $MgSO_4$ as an electrolyte[109]. A poor cycling performance of only 54.3% retention was achieved after 100 cycles at 0.5 A g^{-1}. After the first charging process, the VO_2 anode transformed into stabilized $MgVO_x$, which subsequently served as a host for Mg^{2+} insertion/extraction. In aqueous batteries, the electrochemical performance is severely influenced by temperatures. At low temperatures near the freezing point of electrolytes, lowered interfacial dynamics and ionic conductivity would degrade the performance of the batteries[110]. In aqueous VO_2/δ-MnO_2 batteries, $MgCl_2$ [Figure 6A] effectively disrupts the hydrogen bonding network between water molecules and lowers the freezing point [Figure 6B]. This allows the battery to operate from -50 to 25 °C. However, the issue of active material loss due to partial dissolution leads to poor cycling performance. At 100 mA g^{-1}, 228.5 mAh g^{-1} was achieved at room temperature with retention of 35.4% after 30 cycles, while capacities of 97.9 mAh g^{-1} at -20 °C with retention of 26% and 37.1 mAh g^{-1} at -50 °C with retention of 23% were also attained at the same current rate[111]. Differently, the $Cu_3V_2O_7(OH)_2{\cdot}2H_2O$ cathode lasted for 20,000 cycles with retention of 92% at 10 A g^{-1} besides a high capacity of 262 mAh g^{-1} at 250 mA g^{-1}. The good performance was attributed to intertwined V_6O_{13} layers,

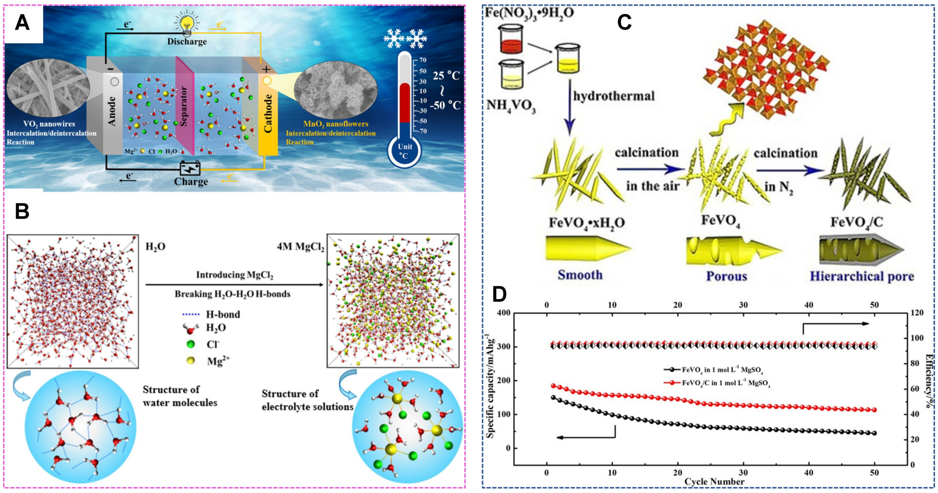

Figure 6. (A) δ-MnO_2//$MgCl_2$ (aq.)//VO_2 operation from 25 to -50 °C and (B) molecule dynamic simulation of water and $MgCl_2$ electrolyte. Reproduced with permission[111]. Copyright 2023, Elsevier. (C) Synthesis of $FeVO_4$/C and (D) relevant cycling performance. Reproduced with permission[112]. Copyright 2017, Wiley-VCH GmbH.

which avails Mg-ion intercalation and stabilizes the structure of $Cu_3V_2O_7(OH)_2 \cdot 2H_2O$[50]. A mesoporous hierarchical $FeVO_4$/C [Figure 6C] anode delivered 184.2 mAh g^{-1} in 1 M $MgSO_4$ electrolyte at 50 mA g^{-1}, and 63.2% capacity was held after 50 cycles [Figure 6D]. The hierarchical pores provide fast pathways for ion diffusion and electrolyte penetration while coating carbon improves the electron conductivity of the anode[112].

Since rechargeable calcium batteries based on organic electrolytes are severely limited in cycling performance and kinetics, Ca-ion batteries with aqueous electrolytes would be an exciting alternative to avoid issues faced by Ca deposition in organic electrolytes and to extend the choice of active materials. An anode material of $CaV_6O_{16} \cdot 7H_2O$ synthesized by a molten salt method exhibited an initial discharge capacity of 208 mAh g^{-1} at 12.5 mA g^{-1}, and a high retention of 97% was obtained after 200 cycles. CVs Cyclic voltammetry curves under different pH values of 2.3 and 10 confirmed that Ca^{2+} intercalation rather than H^+ dominated the energy storage mechanism[113]. A hydrothermally synthesized $K_2V_6O_{16} \cdot 2.7H_2O$ cathode initially discharged 113.9 mAh g^{-1} at 20 mA g^{-1} in a three-electrode aqueous Ca-ion system and held 78.3% capacity after 100 cycles at 50 mA g^{-1}[114]. The comparison of these performances is also summarized in Table 1.

Al-ion batteries

With large theoretical capacity, abundant aluminum resources, and high safety, aqueous aluminum ion batteries have been attractive recently. A layered LiV_3O_8 cathode material delivered 205 mAh g^{-1} in 2 M $Al(CF_3SO_3)_3$ aqueous solution at about 500 mA g^{-1} [Figure 7A] and held 77.3% capacity after 500 cycles[115]. Reversible insertion/extraction of 0.94 mol Al^{3+} per mol LiV_3O_8 was disclosed [Figure 7B]. $FeVO_4$ was converted into $Al_xV_yO_4$ spinel and amorphous Fe-O-Al after Al^{3+} insertion in 1 M $AlCl_3$ aqueous solution. It delivered 350 mAh g^{-1} at 60 mA g^{-1} but decayed rapidly due to vanadium dissolution[116]. The $VOPO_4 \cdot 2H_2O$ nanosheets achieved 125.4 mAh g^{-1} at 20 mA g^{-1}. However, the capacity decreased by 40% after 40 cycles due to the loss of crystal water[117]. A good cycling performance of 2,800 cycles with 86.2% capacity retention was achieved in MoO_3//$VOPO_4$ aluminum ion battery at 1 A g^{-1} when gelatin-polyacrylamide hydrogel electrolyte was used[118]. A novel ultrathin heterostructured nanocomposite of $VOPO_4 \cdot nH_2O$@MXene exhibited 355.7 mAh g^{-1} at 0.5 A g^{-1}, showing a high discharge potential of 1.8 V[62].

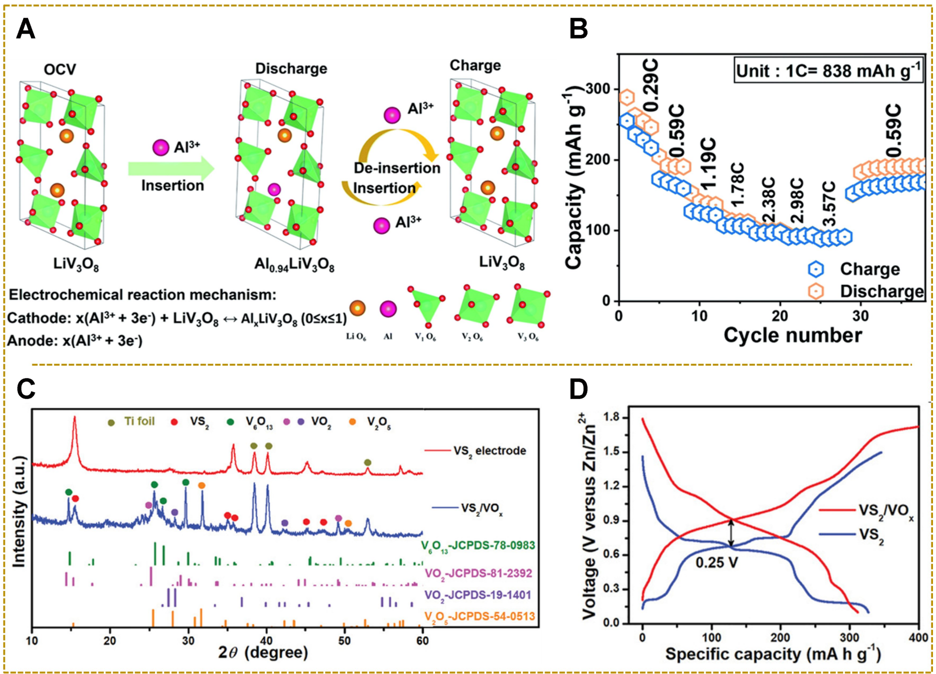

Figure 7. (A) Al^{3+} storage in LiV_3O_8 cathode and (B) Rate performances. Reproduced with permission[115]. Copyright 2022, Elsevier. (C) *Ex situ* XRD characterization of VS_2/VO_x heterostructure and (D) voltage profiles at 1 A g^{-1}. Reproduced with permission[128]. Copyright 2020, Wiley-VCH GmbH.

The bonding of interlayer crystal water and MXenes contributes to extraordinary cycling stability. Table 1 above compares some of the performance.

Mn-ion batteries

Unlike Mg and Al metals with high redox potentials, metal Mn with lower redox potentials is a promising candidate material[119]. Furthermore, Mn has high abundance, good salt solubility, and a small ion radius[120]. All of these indicate that rechargeable aqueous Mn-ion batteries are feasible. However, there are almost no reports on Mn^{2+} carriers in battery research. A $Mn_{0.18}V_2O_5{\cdot}nH_2O$ cathode delivered 83.3 mAh g^{-1} at 5.0 A g^{-1} in 1 M $Mn(CF_3SO_3)_2$ aqueous solution and held 86.7% capacity after 200 cycles at 5.0 A g^{-1}[121]. Yang *et al.* used V_2O_5 as a cathode, sucrose as a water-splitting inhibitor, and sodium perchlorate ($NaClO_4$) and glycine as electrolytes; a strong organic-inorganic interface is formed on Mn metal[119]. The assembled Mn||V_2O_5 battery delivers 180 mAh g^{-1} at 0.5 A g^{-1} and maintains approximately 100% capacity after 200 cycles at 1.5 A g^{-1}.

Zn-ion batteries

Zinc has advantages such as high redox potential, high density, large theoretical volumetric energy density, low cost, and high content[122]. V-based compounds are ideal cathodes for aqueous Zn-ion batteries. The relevant salts used mainly include $ZnCl_2$, $ZnSO_4$, $Zn(CF_3SO_3)_2$, *etc.* Among them, the use of $ZnSO_4$ in V-based Zn-ion batteries readily leads to some electrochemically inactive by-products such as $ZnSO_4(OH)_6{\cdot}xH_2O$ and $Zn_2V_2O_7(OH)_2{\cdot}nH_2O$, which led to depletion of the electrolyte and rapid capacity decay[10,123]. Differently, electrolyte utilizing $Zn(CF_3SO_3)_2$ allows for fast Zn plating/stripping kinetics due to the weak solvation effect of bulky anions[124], but its high price means high cost for large-scale application. Currently, one of the main issues faced by aqueous Zn batteries is the short circuit caused by dendrites generated by the zinc anode[122]. To alleviate this problem, many strategies have been proposed, such as artificial interface layers, 3D structure, alloying, electrolyte engineering, *etc.*[125].

(1) Electrochemical performance

The large interlayer spacings of vanadium sulfides facilitate fast Zn^{2+} diffusion and intercalation. For example, VS_2 delivered 159.3 mAh g^{-1} at 0.1 A g^{-1} in $ZnSO_4$ electrolyte and held 81% capacity at 0.5 A g^{-1} after 200 cycles[126]. A much better performance of 187 mAh g^{-1} at 0.1 A g^{-1} and 85% retention after 2,000 cycles at 2 A g^{-1} was achieved when VS_2 was used as a cathode[127]. A VS_2/VO_x [Figure 7C] heterostructure was reported to deliver 310 mAh g^{-1} with 75% retention after 3,000 cycles. Moreover, the working potential increased by 0.25 V compared with that of pure VS_2 at 1 A g^{-1} [Figure 7D][128]. A VS_2@N-C hybrid with enhanced reactivity and interfacial charge transfer by N-doping delivered 203 mAh g^{-1} at 50 mA g^{-1}, and a retention of 97% was retained after 600 cycles at 1 A g^{-1}[129]. In contrast, VS_4 suffered severe volume changes and dissolution of polysulfides after Zn insertion. Specifically, it was initially converted to $Zn_{3+x}(OH)_2V_2O_7$ in the initial cycles, and Zn^{2+} was subsequently inserted into/ extracted out of the open framework structure reversibly. For example, a flower-like VS_4/carbon nanotubes (CNTs) nanocomposite showed a capacity of 182 mAh g^{-1} at 0.25 A g^{-1} and 93% retention after 1,200 cycles at 5 A g^{-1}[130]. Another VS_4@rGO electrode delivered 180 mAh g^{-1} at 1 A g^{-1} with 93.3% retention after 165 cycles[131].

Vanadium oxides have a wide range of applications in aqueous Zn-ion batteries. V_2O_5 exhibits a theoretical capacity of 589 mAh g^{-1} based on V^{5+}/V^{3+} redox, but the severe deformation accompanying Zn insertion/ extraction readily leads to unstable cycling performance[132]. Proper content of water molecules in interlayers of VO_x polyhedrons avails to shield strong Zn^{2+} host interaction and stabilize the host structure. For example, water molecules in $V_2O_5 \cdot nH_2O$ functioned as a buffer layer, weakening the effective charge of intercalated Zn^{2+}, leading to good rate performance of 248 mAh g^{-1} even at 30 A g^{-1} [Figure 8A][133]. The cycling performance can also be improved with conductive support. A nano paper electrode comprised of V_2O_5 nanofibers and multiwalled CNTs held 168.5 mAh g^{-1} at 10 A g^{-1} for 500 cycles[134]. A nanocomposite with heterostructures of V_2O_5 nanosheets and $Ti_3C_2T_x$ MXenes layer showed enhanced conductivity and robust structure and exhibited stable cycling performance for 5,000 cycles with 99.5% capacity retention at 10 A g^{-1}[41].

Oxygen vacancies usually enhance the conductivity and improve the performance. Dendrites of $V_{10}O_{24} \cdot 12H_2O$, interpreted as $V_2O_{5-x} \cdot nH_2O$ compound with oxygen vacancies, delivered 164.5 mAh g^{-1} at 0.2 A g^{-1} and 3,000 cycles with 80.1% retention at 10 A g^{-1}[135]. After Al doping, structure stability and ion storage capability are highly improved, leading to a high capacity of 534 mAh g^{-1} in Al-doped V_2O_5 at 0.1 A g^{-1}[136]. Relevant theory simulations showed that doping Al significantly reduced the diffusion barrier of Zn^{2+} and increased the conductivity of V_2O_5 [Figure 8B][137].

Corundum-type V_2O_3 with unique channels and suitable pore size distribution shows fast insertion/ extraction of Zn^{2+}[138]. Oxygen-deficient carbon-coated V_2O_3 delivered 662 mAh g^{-1} at 0.2 A g^{-1} [Figure 8C] after turning into $Zn_{0.4}V_2O_{5-m} \cdot nH_2O$ during the first charge [Figure 8D][139]. Similarly, V-deficient V_2O_3 also delivered enhanced Zn-storage capability because vanadium-defect clusters could afford favorable intercalation sites for Zn ions, as revealed by calculations. In addition, intercalated Zn^{2+} at the V vacancies serves as doped heteroatoms, making the host structure more stable [Figure 8E][140].

V_3O_7 with mixed valences (V^{4+}/V^{5+}) provides more active sites[140]. A uniform and ultrafine $V_3O_7 \cdot H_2O$ nano-network delivered 481.3 mAh g^{-1} at 0.1 A g^{-1} [Figure 9A] and 85.4% capacity retention at 5A g^{-1} for 1,000 cycles [Figure 9B][141]. $V_3O_7 \cdot nH_2O$ nanoribbons with rGO exhibited a specific capacity of 410.7 mAh g^{-1}

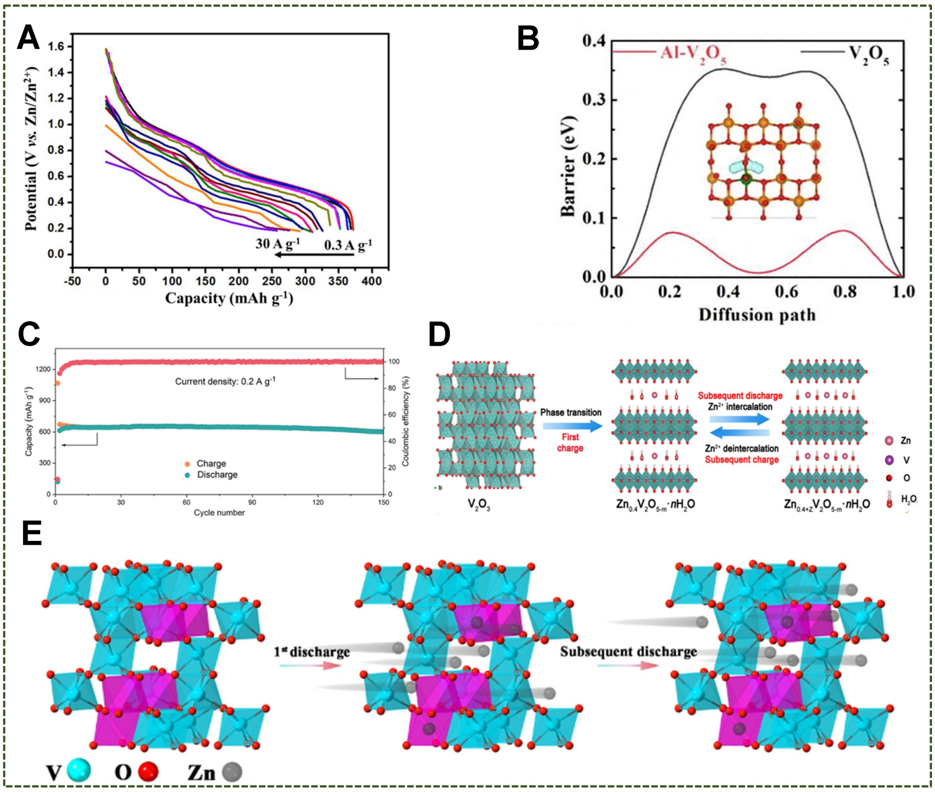

Figure 8. (A) The discharge curves of $V_2O_5{\cdot}nH_2O$ at 0.3-30 A g^{-1}. Reproduced with permission[133]. Copyright 2017, Wiley-VCH GmbH. (B) Diffusion paths in V_2O_5 and Al-V_2O_5. Reproduced with permission[137]. Copyright 2022, Elsevier. (C) Cycling performances and (D) reaction mechanism of V_2O_3. Reproduced with permission[139]. Copyright 2021, American Chemical Society. (E) Energy storage mechanism in the Zn|| V_2O_3 cells. Reproduced with permission under the terms of the Creative Commons Attribution[140]. Copyright 2021, the Author(s), Springer Nature.

at 0.5 A g^{-1} and 99.6% retention at 4 A g^{-1} after 1,000 cycles[142]. Core-shell nanowires of $V_3O_7{\cdot}H_2O@V_2O_5{\cdot}nH_2O$ showed a capacity of 455 mAh g^{-1} at 0.1 A g^{-1} and 85% retention at 0.5 A g^{-1} for 1,200 cycles[143].

Similarly, V_6O_{13} delivered 360 mAh g^{-1} at 0.2 A g^{-1}, benefiting from reduced diffusion barriers of hydrated Zn^{2+} [Figure 9C-E][28]. A 3D nested structure of V_6O_{13} cathodes even exhibited a capacity of 520 mAh g^{-1} at 0.5 A g^{-1} and 85.3% retention at 2 A g^{-1} after 1,000 cycles due to short diffusion depth and large surface[144]. The electrode of V_6O_{13} with trapped CO_2 molecules showed a capacity of 471 mAh g^{-1} at 0.1 A g^{-1} and 80% capacity retention at 2A g^{-1} for 4,000 cycles [Figure 9F] due to significantly reduced relative energy of Zn^{2+} diffusion [Figure 9G][145].

Unlike other vanadium oxides, tunnel-structured VO_2 showed enhanced structural stability, benefiting from shared corner and edge resistance to lattice shearing accompanying ion insertion/extraction[146]. However, low conductivity and instability in acidic aqueous solutions limited its ion storage capability and cycle performance. For example, a capacity of 610 mAh g^{-1} was achieved at 0.1 A g^{-1} by *in situ* electrochemical oxidation of VO_2 nanorods to $V_2O_5{\cdot}nH_2O$[147]. Similar transitions were also observed for monoclinic VO_2[148]. Besides $V_2O_5{\cdot}nH_2O$, VO_2 could also be *in situ* converted into ZnV_2O_7, which showed 408.4 mAh g^{-1} at 0.1 A g^{-1} and 91% retention at 10 A g^{-1} for 4,000 cycles [Figure 10A and B][149]. Moreover, VO_2 with structure defects, such as Mn-doped VO_2, oxygen vacancy-rich VO, *etc.*, also exhibited improved performance[150]. The performance of vanadium oxides could be improved by the preintercalation of some ions. The

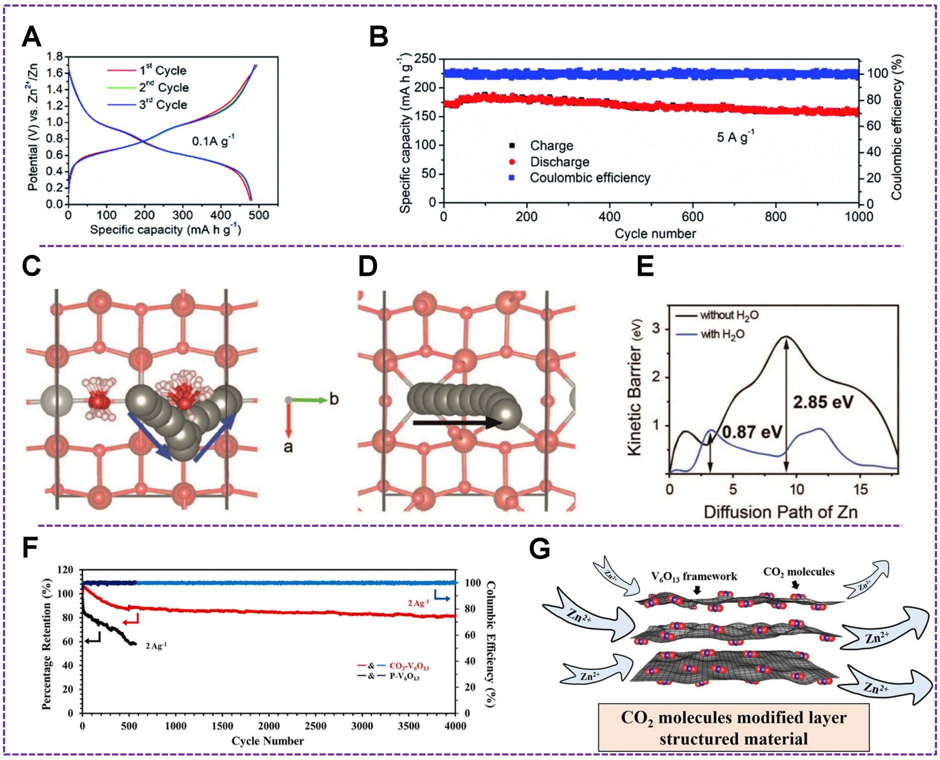

Figure 9. (A) Voltage profiles and (B) long-term cycling stability of $V_3O_7{\cdot}H_2O$ cathode. Reproduced with permission[141]. Copyright 2019, Royal Society of Chemistry. Diffusion paths of Zn ions (C) with and (D) without water and (E) calculated diffusion barriers for paths in (C and D). Reproduced with permission[28]. Copyright 2019, Wiley-VCH GmbH. (F) Cycling performance of Zn//CO_2-V_6O_{13} and Zn//P-V_6O_{13} at 2 A g^{-1} and (G) CO_2 molecules modified layer structured material. Reproduced with permission[145]. Copyright 2021, American Chemical Society.

$Co_{0.247}V_2O_5{\cdot}0.944H_2O$ nanoribbons delivered a capacity of 432 mAh g^{-1} at 0.1 A g^{-1} and 90.26% retention at 10 A g^{-1} after 7,500 cycles [Figure 10C], much better than those of oxide counterparts[151]. Similarly, a $Cu_{0.34}V_2O_5$ cathode delivered 258 mAh g^{-1} at 100 mA g^{-1}[152].

Vanadates are also good candidates for Zn-storage. The layered LiV_3O_8 discharged 200 mAh g^{-1} at 133 mA g^{-1} in an aqueous $ZnSO_4$ electrolyte[153]. A $H_{11}Al_2V_6O_{23.2}$ cathode with an interwoven layer nanosheet structure delivered 288 mAh g^{-1} at 0.1A g^{-1} [Figure 10D] due to short diffusion length and abundant active sites[56]. The $Ag_2V_4O_{11}$ cathode was reported to deliver 213 mAh g^{-1} at 0.2 A g^{-1} and 93% retention at 5 A g^{-1} after 6,000 cycles, benefiting from a pseudo-Zn-air reaction[154]. K^+ can act as pillars between the vanadium-oxygen intercalation layers[138], thus improving the structural stability. A $K_2V_8O_{21}$ cathode exhibited a high capacity of 247 mAh g^{-1} at 0.3 A g^{-1}, and about 128 mAh g^{-1} was retained at 6 A g^{-1} after 300 cycles, corresponding to retention of 83%[87]. A free-standing potassium vanadate/single walled CNTs (KVO/SWCNTs) composite film exhibited a capacity of 379 mAh g^{-1}, and the capacity only decays from 220 to 200 mAh g^{-1} after 10,000 cycles at 5 A g^{-1}[155]. Different cations can synergistically coexist between layers of vanadium oxides. $NaCa_{0.6}V_6O_{16}{\cdot}3H_2O$ nanoribbons with a unique V_3O_8 laminar structure, which energetically favors Zn^{2+} diffusion, delivered 247 mAh g^{-1} at 0.1 A g^{-1} and retained 83% capacity at 5 A g^{-1} after 10,000 cycles[156]. Layered alkali vanadates have an open-framework structure, thus enabling fast Zn^{2+} diffusion. A self-supported membrane of $Zn_3V_2O_7(OH)_2{\cdot}2H_2O$ with a porous crystal structure achieved 213 mAh g^{-1} at 50 mA g^{-1}[157]. A layer $Fe_5V_{15}O_{39}(OH)_9{\cdot}9H_2O$ nanosheet cathode delivered 358 mAh g^{-1} at 0.1 A g^{-1} and 80% retention at 5 A g^{-1} after 300 cycles[158].

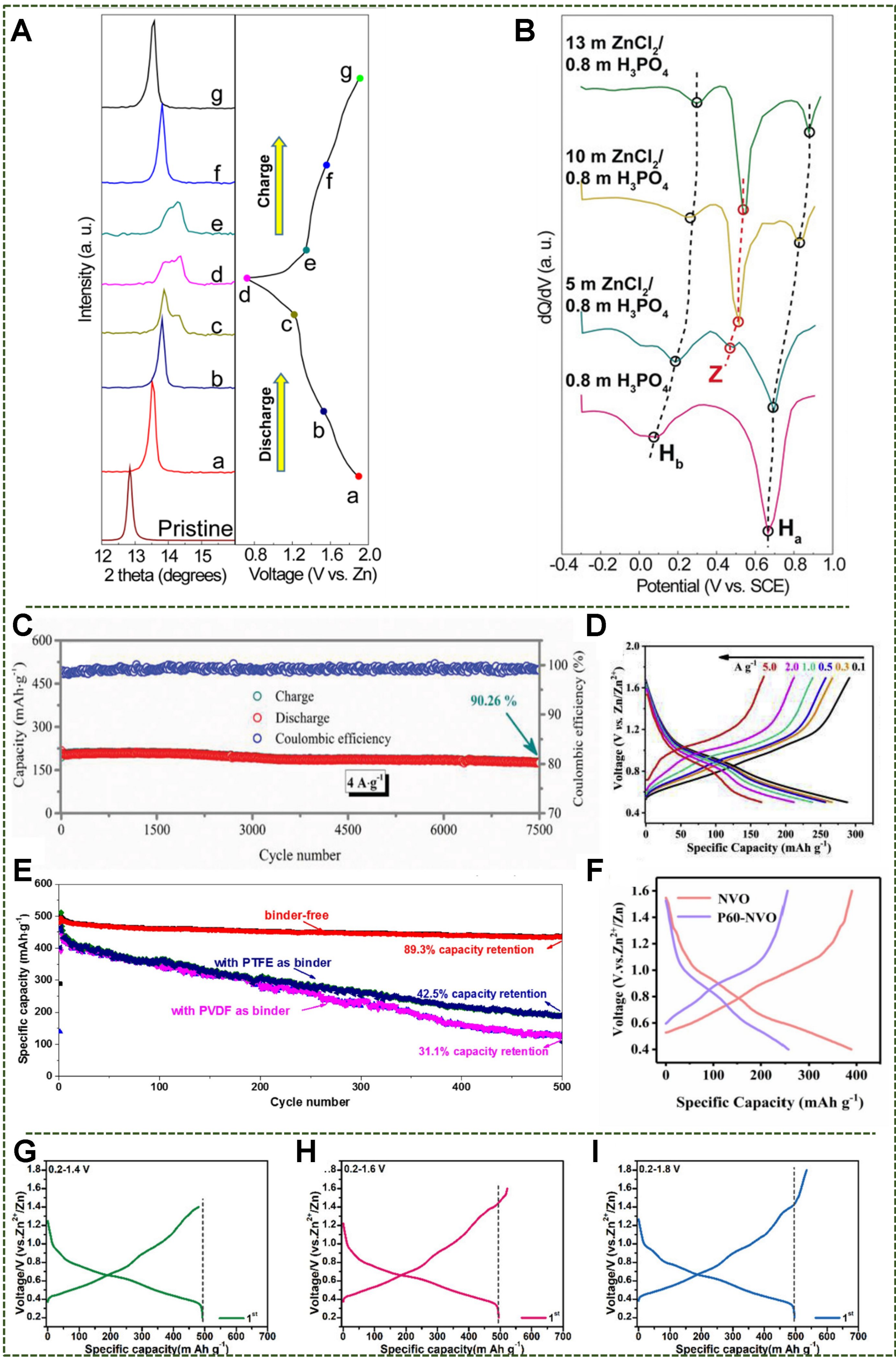

Figure 10. (A) XRD characterization of the VOP cathode at different charge-discharge stages and (B) phase transition disclosed from the differential capacity curve at various concentrations. Reproduced with permission[162]. Copyright 2019, Wiley-VCH GmbH. (C) Cycling performance of $Co_{0.247}V_2O_5{\cdot}0.944H_2O$ at 4 A g^{-1}. Reproduced with permission[151]. Copyright 2019, Wiley-VCH GmbH. (D) Charge-discharge curves of $H_{11}Al_2V_6O_{23.2}$ at 0.1-5.0 A g^{-1}. Reproduced with permission[56]. Copyright 2020, Elsevier. (E) Cycling performance of $(NH_4)_{0.38}V_2O_5$/CNTs paper electrode. Reproduced with permission[160]. Copyright 2021, Elsevier. (F) Typical charge-discharge curves of $NH_4V_3O_8{\cdot}0.5H_2O$ and PANI- $NH_4V_3O_8{\cdot}0.5H_2O$ electrodes at 1 A g^{-1}. Reproduced with permission[57]. Copyright 2022, Elsevier. Typical charge-discharge curves of $NH_4V_4O_{10}$ at (G) 0.2-1.4 V, (H) 0.2-1.6 V, and (I) 0.2-1.8 V. Reproduced with permission under the terms of the Creative Commons Attribution[161]. Copyright 2023, the Author(s), Wiley-VCH GmbH.

The presence of hydrogen bonding between NH_4^+ and V-O layers makes a stable structure in ammonia vanadate, resulting in excellent long-term cycling stability[159]. For example, ultrathin $(NH_4)_2V_{10}O_{25}{\cdot}8H_2O$ nanoribbons, with large interlayer spacings of 1.045 nm favoring fast Zn^{2+} diffusion, achieved 228.8 mAh g^{-1} at 100 mA g^{-1} and 90.1% retention at 5 A g^{-1} after 5,000 cycles[54]. A binder-free cathode of $(NH_4)_{0.38}V_2O_5$ nanoribbons delivered 465 mAh g^{-1} at 100 mA g^{-1}, and the retention was 89.3% after 500 cycles [Figure 10E][160]. An $NH_4V_3O_8{\cdot}0.5H_2O$ and PANI hybrid initially discharged 397.5 mAh g^{-1} at 1A g^{-1} [Figure 10F], benefiting from the tailored large interlayer spacings[57]. The regulation of the larger interlayer spacings was also revealed in $NH_4V_4O_{10}$ nanoribbons by variation of charged voltages or discharge capacities [Figure 10G-I]. When the cathode was charged to 1.6 V, it displayed 223 mAh g^{-1} at 10 A g^{-1} and 97.5% retention after 1,000 cycles[161].

V-based phosphates showed high discharge plateaus due to strong inductive effect of PO_4^{3-} and represented a type of promising high-energy electrode material for Zn-ion batteries[58]. However, they also faced various issues. $VOPO_4{\cdot}nH_2O$ dissolves easily in aqueous solution, leading to poor cycling performance[61]. Concentrated $ZnCl_2$ electrolyte was reported to prevent the dissolution of $VOPO_4{\cdot}2H_2O$ and protect Zn metal from hydrogen evolution reactions and dendrites[162,163]. Additionally, 29 M $ZnCl_2$ was adopted to inhibit H^+ cointercalation and dissolution of $LiV_2(PO_4)_3$[162]. The addition of 70% PEG favored reducing free water in the electrolyte and improving the coulomb efficiency[164]. The presence of high concentration of oxygen vacancies largely improved Zn^{2+} diffusion kinetics in $VOPO_4{\cdot}2H_2O$ nanosheets [Figure 11A]. Mott-Schottky (impedance potential) measurements also showed that the electronic conductivity was greatly improved due to high concentration of O vacancies, which increases the carrier concentration by about 57 times [Figure 11B]. As a result of these unique characteristics, the specific capacity was 313.6 mAh g^{-1} at 0.1 A g^{-1}, and the retention was 76.8% after 500 cycles at 5.0 A g^{-1}[61]. Intercalation of aniline significantly increased the hydrophobicity of $VOPO_4{\cdot}2H_2O$ cathode, thus inhibiting dissolution. Meanwhile, large layer spacing of 16.5 Å and a high diffusion coefficient of 5.7×10^{-8} $cm^{-2}s^{-1}$ were also achieved[165]. An open Na superionic conductor with a stable structure facilitates rapid ion diffusion[166]. Mesoporous graphene oxide-coated $Na_3V_2(PO_4)_2F_3$ nanoparticles [Figure 11C] delivered 126.9 mAh g^{-1} at 0.5 C (1 C = 128 mA g^{-1}) [Figure 11D], showing a very little capacity decay of only 0.0074% per cycle at 15 C for 5,000 cycles [Figure 11E][60]. Table 1 also shows the comparison of the performance.

(2) Energy storage mechanism

Safe and cost-effective aqueous Zn batteries are well-suited for large-scale applications. However, some reaction mechanisms of the cathodes are currently controversial. The dominant mechanisms include reversible intercalation of Zn^{2+}/H^+ or solvated Zn^{2+}/H_2O. Reversible or irreversible phase transitions accompany the ion intercalation process. Various by-products are also generated in the process, such as $Zn_3V_2O_7(OH)_2{\cdot}nH_2O$, $Zn_4SO_4(OH)_6{\cdot}nH_2O$, $Zn_x(OH)_y(CF_3SO_3){\cdot}nH_2O$. The OH^- in $Zn_4SO_4(OH)_6{\cdot}nH_2O$ and $Zn_3V_2O_7(OH)_2{\cdot}nH_2O$ comes from water decomposition in the electrolyte.

$Zn_3V_2O_7(OH)_2{\cdot}nH_2O$ is a very common by-product of aqueous Zn-ion batteries, and there is considerable controversy about the role of $Zn_3V_2O_7(OH)_2{\cdot}nH_2O$ in the battery. For example, when $Fe_2V_4O_{13}$ was used as the cathode, $Zn_3V_2O_7(OH)_2{\cdot}2H_2O$ could reversibly appear and disappear[167]. Partial $Fe_2V_4O_{13}$ converted into $Zn_3V_2O_7(OH)_2{\cdot}2H_2O$ in the discharge. Meanwhile, the remaining acted as a host to store Zn^{2+}. During the subsequent charge process, Zn^{2+} was reversibly extracted, and $Zn_3V_2O_7(OH)_2{\cdot}2H_2O$ reversibly converted into $Fe_2V_4O_{13}$. When V_2O_3 was discharged below 0.8 V in the $Zn(CF_3SO_3)_2$ electrolyte, $Zn_3(OH)_2V_2O_7{\cdot}H_2O$ was formed, while it disappeared when charging to 1.6 V[168]. However, the highly crystalline phase of $Zn_3V_2O_7(OH)_2{\cdot}nH_2O$ electrochemically inactive became dominant when a large amount of it accumulated in aqueous electrolytes[147]. Therefore, excessive accumulation of $Zn_3V_2O_7(OH)_2{\cdot}nH_2O$ would result in poor

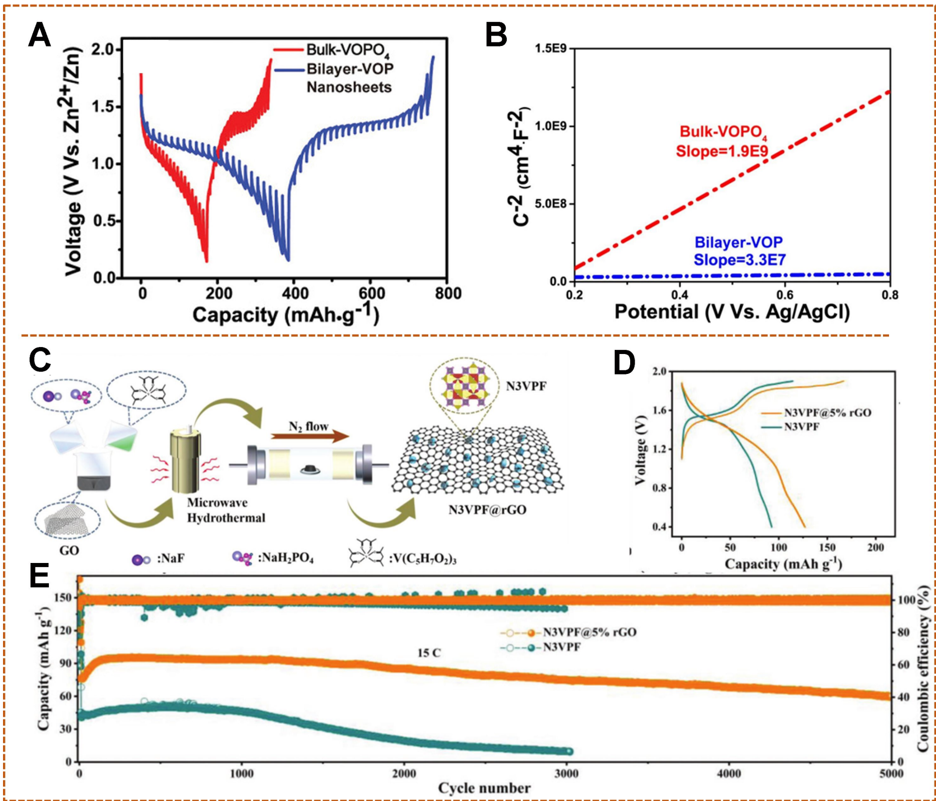

Figure 11. Kinetics in Zn//bulk-$VOPO_4$ and Zn//bilayer-$VOPO_4$ batteries. (A) GITT and (B) Mott-Schottky plots. Reproduced with permission[61]. Copyright 2021, Wiley-VCH GmbH. Material preparation and performance of $Na_3V_2(PO_4)_2F_3$@rGO. (C) Synthesis procedure, (D) galvanostatic charge-discharge profiles at 0.5 C, and (E) Cycling performance at 15 C. Reproduced with permission[60]. Copyright 2023, Wiley-VCH GmbH.

energy storage performance. In contrast, $Zn_{3+x}V_2O_7(OH)_2{\cdot}2H_2O$ derived from VS_4 reflected reversible Zn^{2+} insertion/extraction, while $Zn_3V_2O_7(OH)_2{\cdot}nH_2O$ further transformed to ZnV_3O_8, leading to decay capacity for VS_4@rGO[130].

Coinsertion of Zn^{2+}/H^+ resulted in variation of pH in the electrolyte, contributing to the formation of those by-products, which indirectly proved the insertion/extraction of H^+. For example, ζ-V_2O_5 generated from the $Cu_{0.34}V_2O_5$ cathode after charging to 1.3 V, suffered cointercalation of Zn^{2+} and H^+ accompanying the formation of $(Zn\ (OH)_2)_2(ZnSO_4)\ (H_2O)_n$ [Figure 12A][152]. Reversible H^+ insertion/extraction happened in various cathodes, such as $Cu_{0.18}V_2O_5{\cdot}0.72H_2O$[169], Mn-modified V_6O_{13}[170], $Zn_{0.36}V_2O_5{\cdot}nH_2O$[171], and *etc*., implied by appearance and disappearance of $Zn_4SO_4(OH)_6{\cdot}4H_2O$, $Zn_2V_3O_7(OH)_2{\cdot}2H_2O$, or $Zn_x(OTf)_y(OH)_{2x-y}{\cdot}nH_2O$. Water molecules or hydrogen ions involved in the mechanism were further verified by an organic electrolyte, in which no by-products of $Zn_2V_3O_7(OH)_2{\cdot}2H_2O$ or $Zn_x(OTf)_y(OH)_{2x-y}{\cdot}nH_2O$ were observed.

In hydrated ions, solvation water reduces the effective charge density and increases the distance among neighboring cations, leading to decreased coulomb interactions, which is responsible for the high diffusion coefficient. For example, an interlayer spacing of ~13.2 Å was observed when the hydrated Zn ion was intercalated into a porous $Mg_{0.34}V_2O_5{\cdot}0.84H_2O$ cathode, which was much larger than the size of Zn^{2+} (~0.7 Å) [Figure 12B][45]. CaV_4O_9 exhibited an enhanced charge transfer process due to the cointercalation of Zn^{2+} and H_2O[172]. Similarly, the content of interlayer water in the $Zn_{0.25}V_2O_5{\cdot}nH_2O$ cathode changed with the content of intercalated Zn[38].

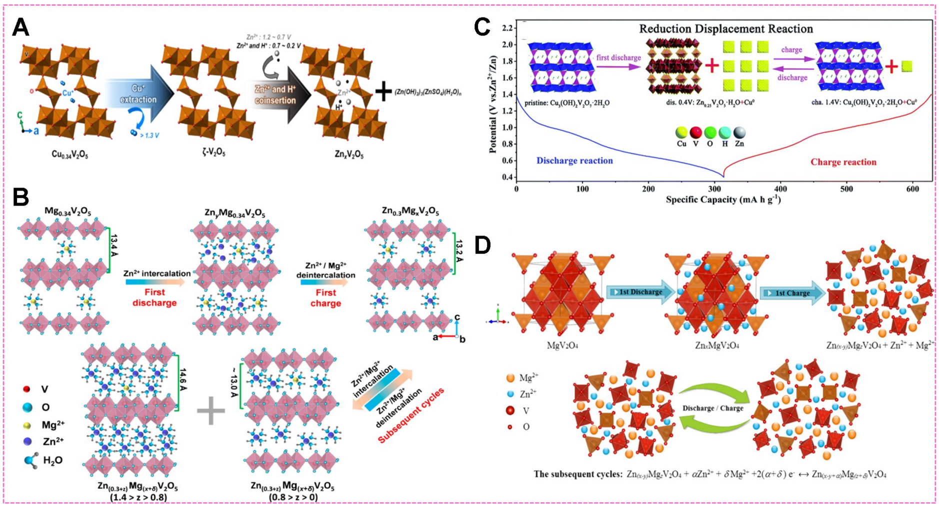

Figure 12. (A) Zn-storage mechanism in $Cu_{0.34}V_2O_5$. Reproduced with permission[152]. Copyright 2021, American Chemical Society. (B) Zn-storage mechanism in $Mg_{0.34}V_2O_5{\cdot}0.84H_2O$. Reproduced with permission[45]. Copyright 2018, American Chemical Society. (C) Reaction mechanism of $Cu_3(OH)_2V_2O_7{\cdot}2H_2O$ at 0.1 A g^{-1}. Reproduced with permission[173]. Copyright 2019, Royal Society of Chemistry. (D) Zn-storage in MgV_2O_4. Reproduced with permission[174]. Copyright 2020, American Chemical Society.

Differently, intercalation of desolvated Zn^{2+} also happened in some circumstances. It was reported that the transformation from Cu^{2+} to metallic Cu^0 particles occurred when desolvated Zn^{2+} intercalated into copper vanadates, e.g., from $Cu_3(OH)_2V_2O_7{\cdot}2H_2O$ to $Zn_{0.25}V_2O_5{\cdot}H_2O$; the processes were verified reversible after Zn extraction [Figure 12C][173]. Moreover, metallic Cu facilitates good electronic conductivity and superior rate capability. In another example, MgV_2O_4 with intercalated Zn formed in the discharge suffered from the extraction of both Zn^{2+} and Mg^{2+} in the charge process. Compared to Zn^{2+}, Mg^{2+} was preferentially extracted. The resultant $Zn_xMgV_2O_4$ [Figure 12D] served as a stable host for reversible Zn-storage, subsequently[174].

Supercapacitors

Compared with batteries, supercapacitors have lower sensitivity to temperature, better tolerance to charge/discharge cycles, superior power performance, and good cycling stability[175]. V-based materials are also considered as promising high-energy electrodes for electrochemical capacitors due to their excellent specific capacitance, long cycling stability, and good electrochemical reversibility[176], but poor electrical conductivity has hindered their further use in supercapacitors. A $VOSO_4$ additive was reported to dramatically improve the cycling stability of V_2O_5-based supercapacitors, leading to 91.23% retention at 10 A g^{-1} after 10,000 cycles[177].

CONCLUSIONS AND FUTURE PROSPECTS

This review combed recent advances of multivalent-ion storage applications for a variety of advanced V-based materials, including vanadium oxides, vanadates, vanadium sulfides, and V-based MXenes and phosphates. The features for typical structures were analyzed with representative materials. The relevant electrochemical properties and energy storage mechanisms for different advanced V-based electrodes were systemically discussed. The discussion covered devices of not only non-aqueous batteries and aqueous batteries but also supercapacitors. For different devices, challenges from poor conductivity, slow ion diffusion, dissolution and structural collapse, low operating voltage, *etc.* were discussed with the corresponding representative electrodes.

Based on the review, we disclosed that issues for V-based materials could be alleviated, to some extent, by common material engineering strategies such as nanosizing, doping, encapsulating, constructing vacancies and heterostructures, *etc*. Further, electrolyte design, e.g., highly concentrated electrolytes, organic/aqueous hybrid electrolytes, hybrid ions electrolytes, *etc*., are also beneficial to improve main factors of structure stability, ion storage capability and diffusion kinetics due to optimized surface/interface, weakened coulomb interactions, and enhanced storage pathways. Overall, to obtain better multivalent-ion storage applications for V-based materials, cooperation from material engineering and electrolyte design is possibly a promising avenue. Meanwhile, various advanced *in-situ* characterization techniques are also needed to clarify the relevant complex interactions between materials and electrolytes.

DECLARATIONS

Authors' contributions

Proposed the topic of this review: Song H, Wang C
Prepared the manuscript: Guo W
Writing - review & editing: Guo W, Fu D, Song H, Wang C

Availability of data and materials

Not applicable.

Financial support and sponsorship

The work is financially supported by the National Natural Science Foundation of China (grant nos. 91963210, 52322107) and the Natural Science Foundation of Guangdong Province (grant nos. 2020B0101690001, 2022A1515010723).

Conflict of interest

All authors declared that there are no conflicts of interest.

Ethical approval and consent to participate

Not applicable.

Consent for publication

Not applicable.

REFERENCES

1. Liu J, Bao Z, Cui Y, et al. Pathways for practical high-energy long-cycling lithium metal batteries. *Nat Energy* 2019;4:180-6. DOI
2. Ren B, Cui H, Wang C. Self-supported graphene nanosheet-based composites as binder-free electrodes for advanced electrochemical energy conversion and storage. *Electrochem Energy Rev* 2022;5:2-27. DOI
3. Song H, Su J, Wang C. The anion-cation relay battery prototype. *Small Sci* 2021;1:2000030. DOI
4. Wu L, Sun R, Xiong F, et al. A rechargeable aluminum-ion battery based on a VS_2 nanosheet cathode. *Phys Chem Chem Phys* 2018;20:22563-8. DOI
5. Canepa P, Sai Gautam G, Hannah DC, et al. Odyssey of multivalent cathode materials: open questions and future challenges. *Chem Rev* 2017;117:4287-341. DOI
6. Song H, Li Y, Tian F, Wang C. Electrolyte optimization and interphase regulation for significantly enhanced storage capability in Ca-metal batteries. *Adv Funct Mater* 2022;32:2200004. DOI
7. Song H, Su J, Wang C. Hybrid solid electrolyte interphases enabled ultralong life Ca-metal batteries working at room temperature. *Adv Mater* 2021;33:e2006141. DOI
8. Song H, Wang C. Current status and challenges of calcium metal batteries. *Adv Energy Sustain Res* 2022;3:2100192. DOI

9. Muldoon J, Bucur CB, Gregory T. Quest for nonaqueous multivalent secondary batteries: magnesium and beyond. *Chem Rev* 2014;114:11683-720. DOI PubMed
10. Tang B, Shan L, Liang S, Zhou J. Issues and opportunities facing aqueous zinc-ion batteries. *Energy Environ Sci* 2019;12:3288-304. DOI
11. Yan Y, Li B, Guo W, Pang H, Xue H. Vanadium based materials as electrode materials for high performance supercapacitors. *J Power Sources* 2016;329:148-69. DOI
12. Xu X, Xiong F, Meng J, et al. Vanadium-based nanomaterials: a promising family for emerging metal-ion batteries. *Adv Funct Mater* 2020;30:1904398. DOI
13. Liu S, Kang L, Kim JM, Chun YT, Zhang J, Jun SC. Recent advances in vanadium-based aqueous rechargeable zinc-ion batteries. *Adv Energy Mater* 2020;10:2000477. DOI
14. Prasadam V, Bahlawane N, Mattelaer F, et al. Atomic layer deposition of vanadium oxides: process and application review. *Mater Today Chem* 2019;12:396-423. DOI
15. Wan F, Niu Z. Design strategies for vanadium-based aqueous zinc-ion batteries. *Angew Chem Int Ed* 2019;58:16358-67. DOI PubMed
16. Xu Y, Deng X, Li Q, et al. Vanadium oxide pillared by interlayer Mg^{2+} ions and water as ultralong-life cathodes for magnesium-ion batteries. *Chem* 2019;5:1194-209. DOI
17. Miao X, Chen Z, Wang N, et al. Electrospun V_2MoO_8 as a cathode material for rechargeable batteries with Mg metal anode. *Nano Energy* 2017;34:26-35. DOI
18. Hu P, Hu P, Vu TD, et al. Vanadium oxide: phase diagrams, structures, synthesis, and applications. *Chem Rev* 2023;123:4353-415. DOI PubMed PMC
19. Zou C, Fan L, Chen R, et al. Thermally driven V_2O_5 nanocrystal formation and the temperature-dependent electronic structure study. *CrystEngComm* 2012;14:626-31. DOI
20. Huie MM, Bock DC, Takeuchi ES, Marschilok AC, Takeuchi KJ. Cathode materials for magnesium and magnesium-ion based batteries. *Coord Chem Rev* 2015;287:15-27. DOI
21. Lee S, Ivanov IN, Keum JK, Lee HN. Epitaxial stabilization and phase instability of VO_2 polymorphs. *Sci Rep* 2016;6:19621. DOI PubMed PMC
22. Wei M, Sugihara H, Honma I, Ichihara M, Zhou H. A New metastable phase of crystallized $V_2O_4 \cdot 0.25H_2O$ nanowires: synthesis and electrochemical measurements. *Adv Mater* 2005;17:2964-9. DOI
23. Chernova NA, Roppolo M, Dillon AC, Whittingham MS. Layered vanadium and molybdenum oxides: batteries and electrochromics. *J Mater Chem* 2009;19:2526. DOI
24. Liu M, Su B, Tang Y, Jiang X, Yu A. Recent advances in nanostructured vanadium oxides and composites for energy conversion. *Adv Energy Mater* 2017;7:1700885. DOI
25. Jin T, Li H, Li Y, Jiao L, Chen J. Intercalation pseudocapacitance in flexible and self-standing V_2O_3 porous nanofibers for high-rate and ultra-stable K ion storage. *Nano Energy* 2018;50:462-7. DOI
26. Yi T, Qiu L, Qu J, Liu H, Zhang J, Zhu Y. Towards high-performance cathodes: design and energy storage mechanism of vanadium oxides-based materials for aqueous Zn-ion batteries. *Coord Chem Rev* 2021;446:214124. DOI
27. Li H, He P, Wang Y, Hosono E, Zhou H. High-surface vanadium oxides with large capacities for lithium-ion batteries: from hydrated aerogel to nanocrystalline VO_2(B), V_6O_{13} and V_2O_5. *J Mater Chem* 2011;21:10999. DOI
28. Shin J, Choi DS, Lee HJ, Jung Y, Choi JW. Hydrated Intercalation for high-performance aqueous zinc ion batteries. *Adv Energy Mater* 2019;9:1900083. DOI
29. Zhang Y, Liu X, Xie G, et al. Hydrothermal synthesis, characterization, formation mechanism and electrochemical property of $V_3O_7 \cdot H_2O$ single-crystal nanobelts. *Mater Sci Eng B* 2010;175:164-71. DOI
30. Lv T, Peng Y, Zhang G, et al. How about vanadium-based compounds as cathode materials for aqueous zinc ion batteries? *Adv Sci* 2023;10:e2206907. DOI PubMed PMC
31. Liu Y, Xu L, Guo X, Lv T, Pang H. Vanadium sulfide based materials: synthesis, energy storage and conversion. *J Mater Chem A* 2020;8:20781-802. DOI
32. Rout CS, Kim BH, Xu X, et al. Synthesis and characterization of patronite form of vanadium sulfide on graphitic layer. *J Am Chem Soc* 2013;135:8720-5. DOI
33. Feng J, Sun X, Wu C, et al. Metallic few-layered VS_2 ultrathin nanosheets: high two-dimensional conductivity for in-plane supercapacitors. *J Am Chem Soc* 2011;133:17832-8. DOI
34. Yao K, Wu M, Chen D, et al. Vanadium tetrasulfide for next-generation rechargeable batteries: advances and challenges. *Chem Rec* 2022;22:e202200117. DOI
35. Hu Z, Liu Q, Chou SL, Dou SX. Advances and challenges in metal sulfides/selenides for next-generation rechargeable sodium-ion batteries. *Adv Mater* 2017;29:1700606. DOI PubMed
36. Sun R, Wei Q, Li Q, et al. Vanadium sulfide on reduced graphene oxide layer as a promising anode for sodium ion battery. *ACS Appl Mater Interfaces* 2015;7:20902-8. DOI
37. Cheng S, Yao K, Zheng K, et al. Self-assembled VS_4 hierarchitectures with enhanced capacity and stability for sodium storage. *Energy Environ Mater* 2022;5:592-8. DOI
38. Kundu D, Adams BD, Duffort V, Vajargah SH, Nazar LF. A high-capacity and long-life aqueous rechargeable zinc battery using a

metal oxide intercalation cathode. *Nat Energy* 2016;1:16119. DOI
39. Yang Y, Tang Y, Liang S, et al. Transition metal ion-preintercalated V_2O_5 as high-performance aqueous zinc-ion battery cathode with broad temperature adaptability. *Nano Energy* 2019;61:617-25. DOI
40. Sarkar S, Banda H, Mitra S. High capacity lithium-ion battery cathode using LiV_3O_8 nanorods. *Electrochim Acta* 2013;99:242-52. DOI
41. Oka Y, Yao T, Yamamoto N. Hydrothermal synthesis and structure refinements of alkali-metal trivanadates AV_3O_8 (A = K, Rb, Cs). *Mater Res Bull* 1997;32:1201-9. DOI
42. Krachodnok S, Haller KJ, Willaims ID. Improved synthesis of alkali metal vanadates using a hydrothermal method. *Eng J* 2012;16:19-28. DOI
43. Wadsley AD. Crystal chemistry of non-stoichiometric pentavalent vandadium oxides: crystal structure of $Li_{1+x}V_3O_8$. *Acta Cryst* 1957;10:261-7. DOI
44. Peng S, Li L, Hu Y, et al. Fabrication of spinel one-dimensional architectures by single-spinneret electrospinning for energy storage applications. *ACS Nano* 2015;9:1945-54. DOI
45. Ming F, Liang H, Lei Y, Kandambeth S, Eddaoudi M, Alshareef HN. Layered $Mg_xV_2O_5{\cdot}nH_2O$ as cathode material for high-performance aqueous zinc ion batteries. *ACS Energy Lett* 2018;3:2602-9. DOI
46. Wang J, Wang J, Jiang Y, et al. $CaV_6O_{16}{\cdot}2.8H_2O$ with Ca^{2+} pillar and water lubrication as a high-rate and long-life cathode material for ca-ion batteries. *Adv Funct Mater* 2022;32:2113030. DOI
47. Li J, Mccoll K, Lu X, et al. Multi-scale investigations of δ-$Ni_{0.25}V_2O_5{\cdot}nH_2O$ cathode materials in aqueous zinc-ion batteries. *Adv Energy Mater* 2020;10:2000058. DOI
48. Liu Y, Li C, Xu J, et al. Electroactivation-induced spinel ZnV_2O_4 as a high-performance cathode material for aqueous zinc-ion battery. *Nano Energy* 2020;67:104211. DOI
49. Tang C, Xiong F, Lan B, et al. Constructing a disorder/order structure for enhanced magnesium storage. *Chem Eng J* 2020;382:123049. DOI
50. Ma XF, Li HY, Zhu X, et al. Switchable and strain-releasable Mg-ion diffusion nanohighway enables high-capacity and long-life pyrovanadate cathode. *Small* 2022;18:e2202250. DOI
51. Liu Y, Li Q, Ma K, Yang G, Wang C. Graphene oxide wrapped CuV_2O_6 nanobelts as high-capacity and long-life cathode materials of aqueous zinc-ion batteries. *ACS Nano* 2019;13:12081-9. DOI
52. Zhu K, Jiang W, Wang Z, et al. Hewettite $ZnV_6O_{16}{\cdot}8H_2O$ with remarkably stable layers and ultralarge interlayer spacing for high-performance aqueous Zn-ion batteries. *Angew Chem Int Ed* 2023;62:e202213368. DOI
53. Yang W, Yang W, Huang Y, Xu C, Dong L, Peng X. Reversible aqueous zinc-ion battery based on ferric vanadate cathode. *Chin Chem Lett* 2022;33:4628-34. DOI
54. Wei T, Li Q, Yang G, Wang C. Highly reversible and long-life cycling aqueous zinc-ion battery based on ultrathin $(NH_4)_2V_{10}O_{25}{\cdot}8H_2O$ nanobelts. *J Mater Chem A* 2018;6:20402-10. DOI
55. Vo TN, Kim H, Hur J, Choi W, Kim IT. Surfactant-assisted ammonium vanadium oxide as a superior cathode for calcium-ion batteries. *J Mater Chem A* 2018;6:22645-54. DOI
56. Wei T, Liu Y, Yang G, Wang C. Aluminum vanadate hollow spheres as zero-strain cathode material for highly reversible and durable aqueous zinc-ion batteries. *Energy Storage Mater* 2020;30:130-7. DOI
57. Li Y, Liu Y, Chen J, et al. Polyaniline intercalation induced great enhancement of electrochemical properties in ammonium vanadate nanosheets as an advanced cathode for high-performance aqueous zinc-ion batteries. *Chem Eng J* 2022;448:137681. DOI
58. Liu C, Massé R, Nan X, Cao G. A promising cathode for Li-ion batteries: $Li_3V_2(PO_4)_3$. *Energy Storage Mater* 2016;4:15-58. DOI
59. Jian Z, Hu YS, Ji X, Chen W. NASICON-structured materials for energy storage. *Adv Mater* 2017;29:1601925. DOI
60. Guan J, Huang Q, Shao L, et al. Polyanion-type $Na_3V_2(PO_4)_2F_3$@rGO with high-voltage and ultralong-life for aqueous zinc ion batteries. *Small* 2023;19:e2207148. DOI
61. Wu Z, Lu C, Ye F, et al. Bilayered $VOPO_4{\cdot}2H_2O$ nanosheets with high-concentration oxygen vacancies for high-performance aqueous zinc-ion batteries. *Adv Funct Mater* 2021;31:2106816. DOI
62. Zheng J, Xu T, Xia G, Cui WG, Yang Y, Yu X. Water-stabilized vanadyl phosphate monohydrate ultrathin nanosheets toward high voltage Al-ion batteries. *Small* 2023;19:e2207619. DOI
63. VahidMohammadi A, Hadjikhani A, Shahbazmohamadi S, Beidaghi M. Two-dimensional vanadium carbide (MXene) as a high-capacity cathode material for rechargeable aluminum batteries. *ACS Nano* 2017;11:11135-44. DOI PubMed
64. Gogotsi Y, Anasori B. The rise of MXenes. *ACS Nano* 2019;13:8491-4. DOI PubMed
65. Qureshi A, Abdelhay AH, Zaidi SA, et al. Emerging trends in niobium, vanadium, and molybdenum based MXenes applications. *Crit Rev Solid State Mater Sci* 2024;49:141-62. DOI
66. Liu Y, Jiang Y, Hu Z, et al. In-situ electrochemically activated surface vanadium valence in V_2C MXene to achieve high capacity and superior rate performance for Zn-ion batteries. *Adv Funct Mater* 2021;31:2008033. DOI
67. Guan J, Shao L, Yu L, et al. Two-dimensional $Mg_{0.2}V_2O_5{\cdot}nH_2O$ nanobelts derived from V_4C_3 MXenes for highly stable aqueous zinc ion batteries. *Chem Eng J* 2022;443:136502. DOI
68. Zhu J, Zhang X, Gao H, et al. VS_4 anchored on Ti_3C_2 MXene as a high-performance cathode material for magnesium ion battery. *J Power Sources* 2022;518:230731. DOI
69. Aurbach D, Lu Z, Schechter A, et al. Prototype systems for rechargeable magnesium batteries. *Nature* 2000;407:724-7. DOI

70. An Q, Li Y, Deog Yoo H, et al. Graphene decorated vanadium oxide nanowire aerogel for long-cycle-life magnesium battery cathodes. *Nano Energy* 2015;18:265-72. DOI
71. Wang J, Tan S, Zhang G, et al. Fast and stable Mg^{2+} intercalation in a high voltage $NaV_2O_2(PO_4)_2F$/rGO cathode material for magnesium-ion batteries. *Sci China Mater* 2020;63:1651-62. DOI
72. Dong H, Liang Y, Tutusaus O, et al. Directing Mg-storage chemistry in organic polymers toward high-energy Mg batteries. *Joule* 2019;3:782-93. DOI
73. Zhao Y, Wang D, Yang D, et al. Superior Mg^{2+} storage properties of VS_2 nanosheets by using an APC-$PP_{14}Cl$/THF electrolyte. *Energy Storage Mater* 2019;23:749-56. DOI
74. Li Z, Ding S, Yin J, Zhang M, Sun C, Meng A. Morphology-dependent electrochemical performance of VS_4 for rechargeable magnesium battery and its magnesiation/demagnesiation mechanism. *J Power Sources* 2020;451:227815. DOI
75. Wang Y, Liu Z, Wang C, et al. Highly branched VS_4 Nanodendrites with 1D atomic-Chain structure as a promising cathode material for long-cycling magnesium batteries. *Adv Mater* 2018;30:e1802563. DOI
76. Ding S, Dai X, Tian Y, et al. Synergy strategy of electrical conductivity enhancement and vacancy introduction for improving the performance of VS_4 magnesium-ion battery cathode. *ACS Appl Mater Interfaces* 2021;13:54005-17. DOI
77. Pei C, Yin Y, Sun R, et al. Interchain-expanded vanadium tetrasulfide with fast kinetics for rechargeable magnesium batteries. *ACS Appl Mater Interfaces* 2019;11:31954-61. DOI
78. Xue X, Chen R, Yan C, et al. One-step synthesis of 2-ethylhexylamine pillared vanadium disulfide nanoflowers with ultralarge interlayer spacing for high-performance magnesium storage. *Adv Energy Mater* 2019;9:1900145. DOI
79. Ding S, Dai X, Li Z, et al. PVP-induced synergistic engineering of interlayer, self-doping, active surface and vacancies in VS_4 for enhancing magnesium ions storage and durability. *Energy Storage Mater* 2022;47:211-22. DOI
80. Mukherjee A, Taragin S, Aviv H, Perelshtein I, Noked M. Rationally designed vanadium pentoxide as high capacity insertion material for Mg-ion. *Adv Funct Mater* 2020;30:2003518. DOI
81. Zuo C, Xiao Y, Pan X, et al. Organic-inorganic superlattices of vanadium oxide@polyaniline for high-performance magnesium-ion batteries. *ChemSusChem* 2021;14:2093-9. DOI
82. Joe YS, Kang MS, Jang G, et al. Intercalation of bilayered V_2O_5 by electronically coupled PEDOT for greatly improved kinetic performance of magnesium ion battery cathodes. *Chem Eng J* 2023;460:141706. DOI
83. Wu D, Zhuang Y, Wang F, Yang Y, Zeng J, Zhao J. High-rate performance magnesium batteries achieved by direct growth of honeycomb-like V_2O_5 electrodes with rich oxygen vacancies. *Nano Res* 2023;16:4880-7. DOI
84. Tang H, Xiong F, Jiang Y, et al. Alkali ions pre-intercalated layered vanadium oxide nanowires for stable magnesium ions storage. *Nano Energy* 2019;58:347-54. DOI
85. Rashad M, Zhang H, Asif M, Feng K, Li X, Zhang H. Low-cost room-temperature synthesis of $NaV_3O_8 \cdot 1.69H_2O$ nanobelts for Mg batteries. *ACS Appl Mater Interfaces* 2018;10:4757-66. DOI
86. Wang X, Zhang X, Zhao G, et al. Ether-water hybrid electrolyte contributing to excellent Mg ion storage in layered sodium vanadate. *ACS Nano* 2022;16:6093-102. DOI
87. Tang B, Fang G, Zhou J, et al. Potassium vanadates with stable structure and fast ion diffusion channel as cathode for rechargeable aqueous zinc-ion batteries. *Nano Energy* 2018;51:579-87. DOI
88. Li C, Wu W, Liu Y, et al. Facilitating Mg^{2+} diffusion in high potential $LixV_2(PO_4)_3$ cathode material with a co-insertion strategy for rechargeable Mg-ion batteries. *J Power Sources* 2022;520:230853. DOI
89. Zhang X, Xu X, Song B, et al. Towards a stable layered vanadium oxide cathode for high-capacity calcium batteries. *Small* 2022;18:e2107174. DOI
90. Jeon B, Kwak HH, Hong S. Bilayered $Ca_{0.28}V_2O_5 \cdot H_2O$: high-capacity cathode material for rechargeable Ca-ion batteries and its charge storage mechanism. *Chem Mater* 2022;34:1491-8. DOI
91. Purbarani ME, Hyoung J, Hong S. Crystal-water-free potassium vanadium bronze ($K_{0.5}V_2O_5$) as a cathode material for Ca-ion batteries. *ACS Appl Energy Mater* 2021;4:7487-91. DOI
92. Adil M, Sarkar A, Sau S, Muthuraj D, Mitra S. Non-aqueous rechargeable calcium-ion batteries based on high voltage zirconium-doped ammonium vanadium oxide cathode. *J Power Sources* 2022;541:231669. DOI
93. Wang Y, Cai J, Han T, et al. In-situ growing polyaniline nano-spine array on $FeVO_4$ nanobelts as high-performance rechargeable aluminum-ion battery cathode. *Appl Surf Sci* 2022;591:153157. DOI
94. Singh S, Bairagi PK, Verma N. Candle soot-derived carbon nanoparticles: an inexpensive and efficient electrode for microbial fuel cells. *Electrochim Acta* 2018;264:119-27. DOI
95. Wang H, Xu Q. Materials design for rechargeable metal-air batteries. *Matter* 2019;1:565-95. DOI
96. Ju S, Ye J, Meng Y, Xia G, Yu X. Pre-lithiated $Li_2V_6O_{13}$ cathode enables high-energy aluminum-ion battery. *Adv Energy Mater* 2022;12:2201653. DOI
97. Xing L, Owusu KA, Liu X, et al. Insights into the storage mechanism of VS_4 nanowire clusters in aluminum-ion battery. *Nano Energy* 2021;79:105384. DOI
98. Han X, Wu F, Zhao R, Bai Y, Wu C. Tremella-like vanadium tetrasulfide as a high-performance cathode material for rechargeable aluminum batteries. *ACS Appl Mater Interfaces* 2023;15:6888-901. DOI PubMed
99. Li Q, Rui X, Chen D, et al. A high-capacity ammonium vanadate cathode for zinc-ion battery. *Nanomicro Lett* 2020;12:67. DOI PubMed PMC

100. Tan H, Chen D, Liu W, et al. Free-standing hydrated sodium vanadate papers for high-stability zinc-ion batteries. *Batteries Supercaps* 2020;3:254-60. DOI
101. Mei Y, Liu Y, Xu W, Zhang M, Dong Y, Qiu J. Suppressing vanadium dissolution in 2D V_2O_5/MXene heterostructures via organic/aqueous hybrid electrolyte for stable zinc ion batteries. *Chem Eng J* 2023;452:139574. DOI
102. Yagi S, Ichitsubo T, Shirai Y, et al. A concept of dual-salt polyvalent-metal storage battery. *J Mater Chem A* 2014;2:1144-9. DOI
103. Sun R, Pei C, Sheng J, et al. High-rate and long-life VS_2 cathodes for hybrid magnesium-based battery. *Energy Storage Mater* 2018;12:61-8. DOI
104. Pei C, Xiong F, Sheng J, et al. VO_2 nanoflakes as the cathode material of hybrid magnesium-lithium-ion batteries with high energy density. *ACS Appl Mater Interfaces* 2017;9:17060-6. DOI
105. Hu X, Peng J, Xu F, Ding M. Rechargeable Mg^{2+}/Li^+, Mg^{2+}/Na^+, and Mg^{2+}/K^+ hybrid batteries based on layered VS_2. *ACS Appl Mater Interfaces* 2021;13:57252-63. DOI
106. Rashad M, Li X, Zhang H. Magnesium/lithium-ion hybrid battery with high reversibility by employing $NaV_3O_8·1.69H_2O$ nanobelts as a positive electrode. *ACS Appl Mater Interfaces* 2018;10:21313-20. DOI
107. Zhao S, Li C, Zhang X, et al. An advanced Ca/Zn hybrid battery enabled by the dendrite-free zinc anode and a reversible calcification/decalcification NASICON cathode. *Sci Bull* 2023;68:56-64. DOI
108. Liang Z, Tian F, Yang G, Wang C. Enabling long-cycling aqueous sodium-ion batteries via Mn dissolution inhibition using sodium ferrocyanide electrolyte additive. *Nat Commun* 2023;14:3591. DOI PubMed PMC
109. Zhang H, Cao D, Bai X. High rate performance of aqueous magnesium-ion batteries based on the δ-MnO_2@carbon molecular sieves composite as the cathode and nanowire VO_2 as the anode. *J Power Sources* 2019;444:227299. DOI
110. Zhao Y, Chen Z, Mo F, et al. Aqueous rechargeable metal-ion batteries working at subzero temperatures. *Adv Sci* 2020;8:2002590. DOI PubMed PMC
111. Yang G, Xu X, Qu G, et al. An aqueous magnesium-ion battery working at -50 °C enabled by modulating electrolyte structure. *Chem Eng J* 2023;455:140806. DOI
112. Zhang H, Ye K, Zhu K, et al. High-energy-density aqueous magnesium-ion battery based on a carbon-coated $FeVO_4$ anode and a Mg-OMS-1 cathode. *Chemistry* 2017;23:17118-26. DOI
113. Liu L, Wu YC, Rozier P, Taberna PL, Simon P. Ultrafast synthesis of calcium vanadate for superior aqueous calcium-ion battery. *Research* 2019;2019:6585686. DOI PubMed PMC
114. Dong L, Xu R, Wang P, et al. Layered potassium vanadate $K_2V_6O_{16}$ nanowires: a stable and high capacity cathode material for calcium-ion batteries. *J Power Sources* 2020;479:228793. DOI
115. Soundharrajan V, Nithiananth S, Lee J, Kim JH, Hwang J, Kim J. LiV_3O_8 as an intercalation-type cathode for aqueous aluminum-ion batteries. *J Mater Chem A* 2022;10:18162-9. DOI
116. Kumar S, Satish R, Verma V, et al. Investigating $FeVO_4$ as a cathode material for aqueous aluminum-ion battery. *J Power Sources* 2019;426:151-61. DOI
117. Pang Q, Yang S, Yu X, et al. Realizing reversible storage of trivalent aluminum ions using $VOPO_4·2H_2O$ nanosheets as cathode material in aqueous aluminum metal batteries. *J Alloys Compd* 2021;885:161008. DOI
118. Wang P, Chen Z, Wang H, et al. A high-performance flexible aqueous Al ion rechargeable battery with long cycle life. *Energy Storage Mater* 2020;25:426-35. DOI
119. Yang Q, Qu X, Cui H, et al. Rechargeable aqueous Mn-metal battery enabled by inorganic-organic interfaces. *Angew Chem Int Ed* 2022;61:e202206471. DOI
120. Nimkar A, Chae MS, Wee S, et al. What about manganese? *ACS Energy Lett* 2022;7:4161-7. DOI
121. Bi S, Wang S, Yue F, Tie Z, Niu Z. A rechargeable aqueous manganese-ion battery based on intercalation chemistry. *Nat Commun* 2021;12:6991. DOI PubMed PMC
122. Liu Y, Lu X, Lai F, et al. Rechargeable aqueous Zn-based energy storage devices. *Joule* 2021;5:2845-903. DOI
123. Guo J, Ming J, Lei Y, et al. Artificial solid electrolyte interphase for suppressing surface reactions and cathode dissolution in aqueous zinc ion batteries. *ACS Energy Lett* 2019;4:2776-81. DOI
124. Zhang N, Cheng F, Liu J, et al. Rechargeable aqueous zinc-manganese dioxide batteries with high energy and power densities. *Nat Commun* 2017;8:405. DOI PubMed PMC
125. Zhang W, Dai Y, Chen R, et al. Highly reversible zinc metal anode in a dilute aqueous electrolyte enabled by a pH buffer additive. *Angew Chem Int Ed* 2023;62:e202212695. DOI PubMed PMC
126. He P, Yan M, Zhang G, et al. Layered VS_2 nanosheet-based aqueous Zn ion battery cathode. *Adv Energy Mater* 2017;7:1601920. DOI
127. Jiao T, Yang Q, Wu S, et al. Binder-free hierarchical VS_2 electrodes for high-performance aqueous Zn ion batteries towards commercial level mass loading. *J Mater Chem A* 2019;7:16330-8. DOI
128. Yu D, Wei Z, Zhang X, et al. Boosting Zn^{2+} and NH^{4+} storage in aqueous media via in-situ electrochemical induced VS_2/VO_x heterostructures. *Adv Funct Mater* 2021;31:2008743. DOI
129. Liu J, Peng W, Li Y, Zhang F, Fan X. A VS_2@N-doped carbon hybrid with strong interfacial interaction for high-performance rechargeable aqueous Zn-ion batteries. *J Mater Chem C* 2021;9:6308-15. DOI
130. Gao S, Ju P, Liu Z, et al. Electrochemically induced phase transition in a nanoflower vanadium tetrasulfide cathode for high-performance zinc-ion batteries. *J Energy Chem* 2022;69:356-62. DOI

131. Qin H, Yang Z, Chen L, Chen X, Wang L. A high-rate aqueous rechargeable zinc ion battery based on the VS_4@rGO nanocomposite. *J Mater Chem A* 2018;6:23757-65. DOI
132. Yoo G, Koo B, An G. Nano-sized split V_2O_5 with H_2O-intercalated interfaces as a stable cathode for zinc ion batteries without an aging process. *Chem Eng J* 2022;434:134738. DOI
133. Yan M, He P, Chen Y, et al. Water-Lubricated Intercalation in $V_2O_5 \cdot nH_2O$ for high-capacity and high-rate aqueous rechargeable zinc batteries. *Adv Mater* 2018;30:1703725. DOI
134. Li Y, Huang Z, Kalambate PK, et al. V_2O_5 nanopaper as a cathode material with high capacity and long cycle life for rechargeable aqueous zinc-ion battery. *Nano Energy* 2019;60:752-9. DOI
135. Wei T, Li Q, Yang G, Wang C. High-rate and durable aqueous zinc ion battery using dendritic $V_{10}O_{24} \cdot 12H_2O$ cathode material with large interlamellar spacing. *Electrochim Acta* 2018;287:60-7. DOI
136. Yang G, Wei T, Wang C. Self-healing lamellar structure boosts highly stable zinc-storage property of bilayered vanadium oxides. *ACS Appl Mater Interfaces* 2018;10:35079-89. DOI
137. Jiang H, Gong W, Zhang Y, et al. Quench-tailored Al-doped V_2O_5 nanomaterials for efficient aqueous zinc-ion batteries. *J Energy Chem* 2022;70:52-8. DOI
138. Zhao Y, Han C, Yang J, et al. Stable alkali metal ion intercalation compounds as optimized metal oxide nanowire cathodes for lithium batteries. *Nano Lett* 2015;15:2180-5. DOI
139. Wang X, Zhang Z, Huang M, Feng J, Xiong S, Xi B. In situ electrochemically activated vanadium oxide cathode for advanced aqueous Zn-ion batteries. *Nano Lett* 2022;22:119-27. DOI
140. Zhu K, Wei S, Shou H, et al. Defect engineering on V_2O_3 cathode for long-cycling aqueous zinc metal batteries. *Nat Commun* 2021;12:6878. DOI PubMed PMC
141. Cao Z, Chu H, Zhang H, et al. An *in situ* electrochemical oxidation strategy for formation of nanogrid-shaped $V_3O_7 \cdot H_2O$ with enhanced zinc storage properties. *J Mater Chem A* 2019;7:25262-7. DOI
142. Cao H, Zheng Z, Norby P, Xiao X, Mossin S. Electrochemically induced phase transition in $V_3O_7 \cdot H_2O$ nanobelts/reduced graphene oxide composites for aqueous zinc-ion batteries. *Small* 2021;17:2100558. DOI
143. Ding Y, Peng Y, Chen S, et al. Hierarchical porous metallic V_2O_3@C for advanced aqueous zinc-ion batteries. *ACS Appl Mater Interfaces* 2019;11:44109-17. DOI
144. He P, Liu J, Zhao X, Ding Z, Gao P, Fan L. A three-dimensional interconnected V_6O_{13} nest with a V^{5+}-rich state for ultrahigh Zn ion storage. *J Mater Chem A* 2020;8:10370-6. DOI
145. Shi W, Yin B, Yang Y, et al. Unravelling V_6O_{13} diffusion pathways via CO_2 modification for high-performance zinc ion battery cathode. *ACS Nano* 2021;15:1273-81. DOI
146. Chen L, Ruan Y, Zhang G, et al. Ultrastable and high-performance Zn/VO_2 battery based on a reversible single-phase reaction. *Chem Mater* 2019;31:699-706. DOI
147. Zhu K, Wu T, Huang K. A high-voltage activated high-erformance cathode for aqueous Zn-ion batteries. *Energy Storage Mater* 2021;38:473-81. DOI
148. Wei T, Li Q, Yang G, Wang C. An electrochemically induced bilayered structure facilitates long-life zinc storage of vanadium dioxide. *J Mater Chem A* 2018;6:8006-12. DOI
149. Tang Z, Zou R, Chen X, Li Z, Lei G. Solvothermal synthesis of VO_2 and in situ electrochemical transformation of $Zn_2V_2O_7$ as cathode for long-life aqueous zinc-ion batteries. *J Power Sources* 2023;569:233006. DOI
150. Deng S, Li H, Chen B, et al. High performance of Mn-doped VO_2 cathode for aqueous zinc-ion batteries: an insight into Zn^{2+} storage mechanism. *Chem Eng J* 2023;452:139115. DOI
151. Ma L, Li N, Long C, et al. Achieving both high voltage and high capacity in aqueous zinc-ion battery for record high energy density. *Adv Funct Mater* 2019;29:1906142. DOI
152. Chae MS, Attias R, Dlugatch B, Gofer Y, Aurbach D. Multifold electrochemical protons and zinc ion storage behavior in copper vanadate cathodes. *ACS Appl Energy Mater* 2021;4:10197-202. DOI
153. Alfaruqi MH, Mathew V, Song J, et al. Electrochemical zinc intercalation in lithium vanadium oxide: a high-capacity zinc-ion battery cathode. *Chem Mater* 2017;29:1684-94. DOI
154. Li Q, Liu Y, Ma K, Yang G, Wang C. In situ Ag nanoparticles reinforced pseudo-Zn-air reaction boosting $Ag_2V_4O_{11}$ as high-performance cathode material for aqueous zinc-ion batteries. *Small Methods* 2019;3:1900637. DOI
155. Wan F, Huang S, Cao H, Niu Z. Freestanding potassium vanadate/carbon nanotube films for ultralong-life aqueous zinc-ion batteries. *ACS Nano* 2020;14:6752-60. DOI PubMed
156. Zhu K, Wu T, Huang K. $NaCa_{0.6}V_6O_{16} \cdot 3H_2O$ as an ultra-stable cathode for Zn-ion batteries: the roles of pre-inserted dual-cations and structural water in V_3O_8 layer. *Adv Energy Mater* 2019;9:1901968. DOI
157. Xia C, Guo J, Lei Y, Liang H, Zhao C, Alshareef HN. Rechargeable aqueous zinc-ion battery based on porous framework zinc pyrovanadate intercalation cathode. *Adv Mater* 2018;30:1705580. DOI
158. Peng Z, Wei Q, Tan S, et al. Novel layered iron vanadate cathode for high-capacity aqueous rechargeable zinc batteries. *Chem Commun* 2018;54:4041-4. DOI
159. Wang X, Xi B, Feng Z, et al. Layered $(NH_4)_2V_6O_{16} \cdot 1.5H_2O$ nanobelts as a high-performance cathode for aqueous zinc-ion batteries. *J Mater Chem A* 2019;7:19130-9. DOI
160. Jiang Y, Wu Z, Ye F, et al. Spontaneous knitting behavior of 6.7-nm thin $(NH_4)_{0.38}V_2O_5$ nano- ribbons for binder-free zinc-ion

batteries. *Energy Storage Mater* 2021;42:286-94. DOI
161. Li S, Yu D, Liu J, et al. Quantitative regulation of interlayer space of $NH_4V_4O_{10}$ for fast and durable Zn^{2+} and NH^{4+} storage. *Adv Sci* 2023;10:e2206836. DOI PubMed PMC
162. Shi HY, Song Y, Qin Z, et al. Inhibiting $VOPO_4 \cdot xH_2O$ decomposition and dissolution in rechargeable aqueous zinc batteries to promote voltage and capacity stabilities. *Angew Chem Int Ed* 2019;58:16057-61. DOI
163. Zhang W, Dong M, Jiang K, et al. Self-repairing interphase reconstructed in each cycle for highly reversible aqueous zinc batteries. *Nat Commun* 2022;13:5348. DOI PubMed PMC
164. Li C, Kingsbury R, Zhou L, Shyamsunder A, Persson KA, Nazar LF. Tuning the solvation structure in aqueous zinc batteries to maximize Zn-ion intercalation and optimize dendrite-free zinc plating. *ACS Energy Lett* 2022;7:533-40. DOI
165. Hu L, Wu Z, Lu C, Ye F, Liu Q, Sun Z. Principles of interlayer-spacing regulation of layered vanadium phosphates for superior zinc-ion batteries. *Energy Environ Sci* 2021;14:4095-106. DOI
166. Hu P, Zhu T, Wang X, et al. Aqueous $Zn//Zn(CF_3SO_3)_2//Na_3V_2(PO_4)_3$ batteries with simultaneous Zn^{2+}/Na^+ intercalation/de-intercalation. *Nano Energy* 2019;58:492-8. DOI
167. Pang Q, Sun C, Yu Y, et al. $H_2V_3O_8$ nanowire/graphene electrodes for aqueous rechargeable zinc ion batteries with high rate capability and large capacity. *Adv Energy Mater* 2018;8:1800144. DOI
168. Chen X, Kong Q, Wu X, et al. V_2O_3@C optimized by carbon regulation strategy for ultra long-life aqueous zinc-ion batteries. *Chem Eng J* 2023;451:138765. DOI
169. Ren J, Hong P, Ran Y, Chen Y, Xiao X, Wang Y. Binder-free three-dimensional interconnected $CuV_2O_5 \cdot nH_2O$ nests as cathodes for high-loading aqueous zinc-ion batteries. *Inorg Chem Front* 2022;9:792-804. DOI
170. Li X, Li M, Yang Q, et al. In situ electrochemical synthesis of MXenes without acid/alkali usage in/for an aqueous zinc ion battery. *Adv Energy Mater* 2020;10:2001791. DOI
171. Zhang X, Xue F, Sun X, et al. High-capacity zinc vanadium oxides with long-term cyclability enabled by in-situ electrochemical oxidation as zinc-ion battery cathode. *Chem Eng J* 2022;445:136714. DOI
172. Du Y, Wang X, Zhang Y, et al. High mass loading CaV_4O_9 microflowers with amorphous phase transformation as cathode for aqueous zinc-ion battery. *Chem Eng J* 2022;434:134642. DOI
173. Shan L, Zhou J, Han M, et al. Reversible Zn-driven reduction displacement reaction in aqueous zinc-ion battery. *J Mater Chem A* 2019;7:7355-9. DOI
174. Tang W, Lan B, Tang C, et al. Urchin-like spinel MgV_2O_4 as a cathode material for aqueous zinc-ion batteries. *ACS Sustain Chem Eng* 2020;8:3681-8. DOI
175. Salanne M, Rotenberg B, Naoi K, et al. Efficient storage mechanisms for building better supercapacitors. *Nat Energy* 2016;1:16070. DOI
176. Guo J, Li L, Luo J, et al. Polypyrrole-assisted nitrogen doping strategy to boost vanadium dioxide performance for wearable nonpolarity supercapacitor and aqueous zinc-ion battery. *Adv Energy Mater* 2022;12:2201481. DOI
177. Lee Y, Yoo G, Jo Y, An H, Koo B, An G. Interfacial electrochemical media-engineered tunable vanadium zinc hydrate oxygen defect for enhancing the redox reaction of zinc-ion hybrid supercapacitors. *Adv Energy Mater* 2023;13:2300630. DOI
178. Fu Q, Wu X, Luo X, et al. High-voltage aqueous Mg-ion batteries enabled by solvation structure reorganization. *Adv Funct Mater* 2022;32:2110674. DOI
179. Wu D, Zeng J, Hua H, Wu J, Yang Y, Zhao J. NaV_6O_{15}: a promising cathode material for insertion/extraction of Mg^{2+} with excellent cycling performance. *Nano Res* 2020;13:335-43. DOI
180. Tang H, Chao F, Chen H, et al. Water-lubricated aluminum vanadate for enhanced rechargeable magnesium ion storage. *Small* 2022;18:e2203525. DOI
181. Deng X, Xu Y, An Q, et al. Manganese ion pre-intercalated hydrated vanadium oxide as a high-performance cathode for magnesium ion batteries. *J Mater Chem A* 2019;7:10644-50. DOI
182. Xu X, Duan M, Yue Y, et al. Bilayered $Mg_{0.25}V_2O_5 \cdot H_2O$ as a stable cathode for rechargeable Ca-ion batteries. *ACS Energy Lett* 2019;4:1328-35. DOI
183. Chae MS, Setiawan D, Kim HJ, Hong ST. Layered iron vanadate as a high-capacity cathode material for nonaqueous calcium-ion batteries. *Batteries* 2021;7:54. DOI
184. Gao W, Michalička J, Pumera M. Hierarchical atomic layer deposited V_2O_5 on 3D printed nanocarbon electrodes for high-performance aqueous zinc-ion batteries. *Small* 2022;18:e2105572. DOI PubMed
185. Li Z, Ren Y, Mo L, et al. Impacts of oxygen vacancies on zinc ion intercalation in VO_2. *ACS Nano* 2020;14:5581-9. DOI
186. Chen H, Chen L, Meng J, et al. Synergistic effects in V_3O_7/V_2O_5 composite material for high capacity and long cycling life aqueous rechargeable zinc ion batteries. *J Power Sources* 2020;474:228569. DOI
187. He D, Peng Y, Ding Y, et al. Suppressing the skeleton decomposition in Ti-doped $NH_4V_4O_{10}$ for durable aqueous zinc ion battery. *J Power Sources* 2021;484:229284. DOI
188. He P, Yan M, Liao X, Luo Y, Mai L, Nan C. Reversible V^{3+}/V^{5+} double redox in lithium vanadium oxide cathode for zinc storage. *Energy Storage Mater* 2020;29:113-20. DOI
189. He P, Zhang G, Liao X, et al. Sodium ion stabilized vanadium oxide nanowire cathode for high-performance zinc-ion batteries. *Adv Energy Mater* 2018;8:1702463. DOI

190. Yi H, Zuo C, Ren H, et al. Structure evolution and energy storage mechanism of $Zn_3V_3O_8$ spinel in aqueous zinc batteries. *Nanoscale* 2021;13:14408-16. DOI
191. Li W, Wang K, Cheng S, Jiang K. A long-life aqueous Zn-ion battery based on $Na_3V_2(PO_4)_2F_3$ cathode. *Energy Storage Mater* 2018;15:14-21. DOI